Factors influencing magmatism during continental break-up: new insights from a wide-angle seismic experiment across the conjugate Seychelles-Indian margins

Collier[1*], J.S., Minshull[2], T.A., Hammond[3], J.O.S., Whitmarsh[2], R.B, Kendall[3], J.-M, Sansom[1], V., Lane[2], C.I., Rumpker[4], G.

[1] *Department of Earth Science & Engineering, Imperial College London, UK*
[2] *National Oceanography Centre, University of Southampton, UK*
[3]*Department of Earth Sciences, Bristol University, UK*
[4]*Arbeitsbereich Geophysik, Johann Wolfgang Goethe Universitat, Frankfurt am Main, Germany*

**corresponding author*
Department of Earth Science and Engineering, Imperial College London, SW7 2AZ, UK
email: jenny.collier@ic.ac.uk; Tel: 44 20 7594 6443; Fax: 44 20 7594 7444

1

Abstract

We present a model of the northern Seychelles continental margin derived from controlled-source wide-angle seismic travel-time inversion and teleseismic receiver functions. This margin has been widely cited as a classic example of rifting in association with a continental flood basalt province, the Deccan Traps. However we do not find the typical set of geophysical characteristics reported at other margins linked to continental flood basalts, such as those of the north Atlantic. The oceanic crust formed immediately after break-up and throughout the first 3 Ma of seafloor spreading is just 5.2 km thick, less than half that typically seen at other volcanic margins. The continent-ocean transition zone is narrow and whilst two packages of seaward-dipping-reflectors are imaged within this transition they are weakly developed. Beneath the thinned continental crust there is an approximately 4 km thick layer of high-velocity material (7.5-7.8 km/s) that we interpret as mafic material intruded and underplating the lower crust. However we believe that this underplating most likely happened prior to the break-up. Overall the observations show that that rifting of India from the Seychelles was characterised by modest magmatism. The spatial extent of the Deccan flood basalt province is therefore smaller than previously thought. We speculate that either the lateral flow of Deccan-related hot material beneath the break-up region was hampered, perhaps as the rifted margins did not intersect the centre of the Deccan source, or there was incomplete melt extraction from the wide melting region that formed between the rapidly diverging plates. If the latter explanation is correct then the rate of plate separation, as indicated by the initial seafloor spreading rate, is more important in controlling the volume of magmatism generated during continental rifting than has been previously recognised.

Index terms: 8105, 3025, 8120, 8137, 8178

Keywords: Volcanic continental margins, rifting, magmatism, Seychelles, Deccan.

1 Introduction

In the 1980s and 1990s, studies of rifted continental margins established two-end member types depending on the degree of rift-related magmatism, the so-called volcanic and non-volcanic margins (*Mutter et al.*, 1988; *White*, 1992a). Volcanic margins are characterized by seaward-dipping reflectors corresponding to thick subaerial and shallow-marine lava flows, high seismic velocity (>7.2 km/s) bodies in the lower crust, formed by igneous rocks that intruded and/or underplated the thinned continental crust and thick early oceanic crust (up to twice the normal ca. 7 km thickness for the first ca. 5 Ma of seafloor spreading). In contrast, non-volcanic margins are characterised by 5-20 km wide, tilted, continental blocks bounded by large seaward-dipping normal faults, areas of exhumed sub-continental mantle (*Whitmarsh et al.*, 2001) and/or thin early oceanic crust. Many volcanic margins were shown to be spatially and temporally linked to onshore flood basalt provinces and offshore, to aseismic ridges linking them to present-day hot-spots. Based on this association, it was suggested that the excess magmatism could be entirely explained by decompression melting of passively upwelling hot asthenosphere –or mantle plume head– beneath the thinning lithosphere (*White and McKenzie*, 1989). In the north Atlantic, the region where many of the current ideas about continental break-up developed, the application of this passive-melting model to explain the observed melt volumes implies that the Iceland plume increased mantle temperatures by 150^0C along a 2000 km length of rift (*Barton and White*, 1997). Following break-up, elevated temperatures were maintained only in the ca. 200 km wide immediate plume region to form the Greenland-Iceland-Faeroe ridge, and elsewhere the thermal anomaly decayed and the oceanic crust thickness reached normal values after 5-10 Ma. It has been suggested that this decay might be explained by the presence at breakup time of an exhaustible hot layer at the top of the asthenosphere (*Nielsen and Hopper*, 2004; *Armitage et al.*, 2008).

However not all volcanic margins have conclusive evidence for the presence of a mantle plume at the time of rifting, most notably the Australian Cuvier margin (*Hopper et al.*, 1992) and Eastern United

States margins (*Holbrook et al.,* 1994a; *Holbrook et al.,* 1994b). These examples led to a second group of models in which the excess volcanism was explained by small-scale convection in the upper mantle generated at the time of rifting, without the need for a mantle thermal anomaly at all. Active upwelling increases the throughput of asthenosphere and hence the volume of melt generated by decompression partial melting (*Mutter et al.,* 1988; *van Wijk et al.,* 2001). The proponents of this model argued that it better explained the transient nature of the magmatic anomaly and suggested that the generation of local convection is encouraged by rapid rifting and a narrow rift zone – both thought to be characteristics of volcanic as opposed to non-volcanic margins. Unfortunately, whilst there have been many attempts to generate small-scale convection by numerical simulations, a consensus as to the conditions required to initiate it has not been reached (*Sleep*, 2007). More recently, other workers have proposed a third scenario, in which decompression melting of passively upwelling warm asthenosphere and active convection act *together* to produce the observed excess magmatism (*Kelemen and Holbrook*, 1995; *Keen and Boutilier*, 2000). Applying this idea to the case of the north Atlantic margins, *Holbrook et al.*, (2001) estimated the mantle temperature was just 100^0C hotter than normal beneath the entire province, but with significant active upwelling within 300 km of the Iceland plume compared to only passive upwelling in the more distal regions.

In this paper we present results from a seismic experiment conducted across the north Seychelles continental margin carried out as part of a larger study of the conjugate north Seychelles-Laxmi Ridge margins (Fig.1a). The western Indian continental margin, was one of the first to reveal seaward-dipping reflectors (*Hinz*, 1981), and the rifting of the Seychelles from the Indian sub-continent has been widely linked to the eruption of the Deccan Trap flood basalt province at 65.5 ± 1Ma (*Courtillot and Renne*, 2003). The origin of the Deccan has been attributed to both a mantle plume (that later built the Chagos-Laccadive and Mascarene ridges and to-day resides below Réunion, *Richards et al.*, 1989; *White and McKenzie*, 1989; *Duncan et al.*, 1990) and edge-driven convection induced by lateral variations in lithospheric thickness beneath the Indian subcontinent and surrounding ocean basins (*Anderson*, 1994). The timing of flood basalt emplacement and break-up are well constrained

(*Collier et al.*, 2008) and, irrespective of the origin of the Deccan traps, our study area is a clear, undisputed example of associated continental flood basalt province and continental rifting. The Seychelles-Indian margins therefore provide an ideal opportunity to test our current understanding of the factors which influence the volumes of magma generated during continental break-up that have been largely developed from observations in the Atlantic.

2 The study area

Spectacular exposures of granite led *Wegener* (1924) to first propose that the Seychelles islands and plateau were of continental origin. This was confirmed in the late 1950s/early 1960's when seismic refraction profiles collected with sonobuoys found a thick crust with a continental-like velocity profile that was surrounded by oceanic crust on three sides (*Gaskell et al.*, 1958; *Shor and Pollard*, 1963; *Davies and Francis*, 1964; *Francis et al.*, 1966; *Francis and Shor*, 1966. Fig.1b). No crustal-scale controlled-source seismology has been conducted in the region since this time, and the crustal affinity of the part of the Mascarene Plateau that lies to the south-east of the Seychelles Plateau remains unknown. The Mesozoic sediments on the Seychelles plateau itself however were more recently the focus of hydrocarbon exploration activity that resulted in the collection of an extensive seismic reflection and magnetic dataset and the drilling of four deep wells (*Plummer*, 1994).

The geographic isolation of the Seychelles resulted from three phases of rifting: firstly by the opening of the Western Somali Basin in the mid-Jurassic (~160 Ma), secondly by the opening of the Mascarene Basin in the mid-Cretaceous (~84 Ma) and finally by the opening of the Eastern Somali Basin/Arabian Sea at the end of the Late Cretaceous (~62 Ma, *Norton and Sclater*, 1979). At the time of this final rifting phase, current plate reconstructions of the north Indian Ocean place the Seychelles plateau adjacent to the section of the Indian-Pakistan continental margin known as the Laxmi Ridge (*Todal and Edholm*, 1998; *Royer et al.*, 2002, Fig.1c). The Laxmi Ridge, with its distinctive 25-50 mGal negative free-air gravity anomaly, was first identified by *Naini and Talwani* (1982) who

proposed that it was also a continental fragment that rifted from mainland India by the opening of the Gop Rift prior to rifting from the Seychelles.

Our preferred plate reconstruction (*Royer et al.*, 2002), which accounts for ridge propagation events at the Carlsberg ridge and hence seafloor spreading asymmetry in the Eastern Somali Basin and Arabian Sea, aligns the northwestern tips of the Laxmi Ridge and Seychelles plateau (Fig.1c). This alignment is consistent with the inferred presence of a major transform plate boundary between Greater India (India+Seychelles) and the African plate at this location in the Late Cretaceous (*Plummer*, 1996). The reconstruction also matches three clear segments of seafloor spreading anomaly 27n immediately north of the Seychelles and south of the Laxmi Ridge (*Collier et al.*, 2008). We therefore believe this reconstruction to be an accurate representation of the break-up geometry, and it places our study area approximately 1000 km from the eruptive centre of the Deccan, as inferred by *Hooper* (1990). We estimate that the uncertainty in the position of the Deccan centre is less than ±100 km in the direction of our study area because of the requirement to fit with the location of the offshore Laccadive Ridge to the south, which in both plume and non-plume models is considered to have formed from the Deccan source. Therefore, by analogy with the margins that border the north Atlantic, we would expect the Seychelles margin to display distal volcanic margin characteristics.

Our investigation of the north Seychelles margin was conducted in three distinct phases – swath/magnetic reconnaissance in 2001 (RRS Charles Darwin cruise 134b), the main controlled-source seismic experiment in 2003 (RRS Charles Darwin cruise 144) and passive seismic recording in 2003-4 (*Hammond et al.*, 2005). During the main, controlled-source stage of our study both the Seychelles margin and the conjugate Laxmi Ridge margin were surveyed. In this paper we present the Seychelles wide-angle results. Wide-angle results from the Laxmi Ridge margin are presented by *Minshull et al.*, (2008). An analysis of the seismic reflection and magnetic data collected at the Seychelles margin in 2001 and 2003 is given by *Collier et al.*, (2008).

3 Data acquisition and processing

3.1 Wide-angle data

The ship tracks of our 2003 Seychelles experiment are shown in Fig.2. The main seismic transect (lines 7 and 9) was sited to avoid offsets in seafloor magnetic anomalies and a number of small deep-water seamounts, and extends from seaward of magnetic anomaly 27n in the north, up the bathymetric slope and onto the shallow Seychelles Plateau in the south. Much of the plateau is uncharted, and so for navigational safety coupled with environmental reasons it was necessary to slightly deviate from the optimal line during shooting (line 7). This deviation was taken into account during subsequent data analysis, by excluding arrival picks affected by three-dimensional geometry/structure. The main transect was complemented by 650 km of additional multichannel reflection profiles (lines 10-21, Fig.2).

The wide-angle transect was collected with a 6920 cubic inch, 14-element tuned airgun array designed to be rich in 5-10 Hz energy, fired at 2000 psi every 60 s (every 150 m at a nominal ship speed of 4.5 knots) and towed at 16 m depth. The shots were recorded by 32 Geomar ocean bottom instruments (*Flueh and Bialas*, 1996), consisting of 11 ocean-bottom hydrophones (OBH) and 21 ocean bottom seismometers (OBS) equipped with a 4.5 or 15 Hz, three-component geophone plus hydrophone package, positioned 8 km apart. The conjugate Laxmi Ridge profile was collected first, so the Seychelles OBS/H stations are numbered 33-64. All deployed instruments were recovered, and only one failed to record any data (OBH37). The data were recorded with a 10 ms sample interval and had a correction for clock drift applied. The water column sound-speed profile was measured with a velocimeter to a depth of 4.3 km, and supplemented with shallow water temperature profiles collected by disposable XBTs. Travel time picks of the direct wave were used to calculate the seabed instrument positions. These calculations were done in two-dimensions, so any offline drift was not corrected for. However, the differences between the calculated (relocated) and logged shipboard-drop positions were all less than 100 m, indicating minimal drift during instrument descent and so negligible error. The

final record sections had a 1-20 Hz bandpass filter and a linear offset-dependant gain applied to boost the amplitude of the farthest-offset arrivals.

Due to the probability of high surf noise it was decided not to deploy any seabed instruments on the plateau. Instead here we used two Sparton Electronics AN/SSQ-57A disposable sonobuoys (stations SB09 and SB11), and temporary landstations on the Seychelles Islands of Mahé (stations 01, 04 and 07), Praslin (station 10) and Denis (station 19). The former two are granitic islands in the middle of the plateau, and the latter a coralline cay on the outer shelf. In order to ensure a common time-base between the landstation and ship's GPS clocks the two were cross-synchronised at the end of the cruise and found to be within 0.01ms.

Once the record sections for each land and marine station had been produced, travel time picks of coherent phases were made manually approximately every 1.5 to 3 km (8-16 traces). For the OBS instruments picking was mostly done on the hydrophone components as they generally had better signal-to-noise ratio than the vertical geophones. In places the first water bottom multiple arrivals have higher amplitudes than their equivalent primaries, and were used to guide the picking. Picking of arrivals on the landstation records was similarly aided by the data recorded during the shooting of the other seismic lines parallel to the main transect. On the co-incident multichannel seismic profile the Moho reflection was widely seen as a band of diffuse, high reflectivity up to 0.3 s TWT thick at about 8 s TWT (Fig.3b, Fig.9a). Synthetic zero-offset picks of both the top basement and Moho reflections into seabed instruments 33-61 were calculated from this profile and included with the other travel-time picks. On some of the instruments, helped by this zero-offset guide, it was also possible to pick the wide-angle reflection from top basement where it cross-cut the direct wave reverberation. Travel time uncertainties of up to 250 ms were assigned to each pick by eye according to phase continuity and ambient noise levels, and in general increase with range. The minimum picking error was taken to be 30 ms, a quarter wavelength of the dominant 7.5 Hz signal. The average travel time pick uncertainty

(t_{unc}) for each phase is given in Table 1. During the modelling process, the travel-time picks and assigned uncertainties were checked by travel time reciprocity to ensure internal consistency (*Zelt*, 1999). This method identifies reversed shot and receiver pairs, and is a rapid way of highlighting data mis-picks and/or inappropriate uncertainties. This proved particularly helpful for instruments sited on the relatively steep seafloor immediately north of the plateau (instruments 62-64), where the seabed is disturbed by sediment slumps and slides and some irregularities in the arrival times of short-range events were detected (Fig.3b). The assigned uncertainties were increased in these areas.

3.2 Receiver functions

Following the controlled source part of the experiment, the landstations were reconfigured and left to record teleseismic events for a further 12 months (February 2003 to February 2004, *Hammond et al.*, 2005). During this period a total of 34 earthquake events within an epicentral distance range of 40-90^0 were recorded. In addition we used 87 events recorded at the permanent station of MSEY on the main island of Mahé (station 04) between 1995 and 2005. Receiver functions were computed with an extended time multi-taper method (*Helffrich*, 2006). This method uses multi-taper correlation in the deconvolution step, which prevents spectral leakage and down-weights the noisy parts of the spectrum, an important consideration at island settings such as the Seychelles. The shear-wave structure beneath each station to a depth of 200 km was then established by a combination of *H-κ* stacking (*Zhu and Kanamori*, 2000) and forward modelling (*Langston*, 1979; *Randall*, 1989). The *H-κ* stacking indicated a Vp/Vs ratio of 1.78 for the crust, and so this value was used to convert the final receiver-function derived S-wave velocity models to P-wave velocity models. Further details are given in *Hammond et al.*, submitted.

4 Model development

A 2D isotropic P-wave velocity model for the crust and uppermost mantle was developed using a combination of forward modelling and inversion using the ray-theoretical programs FAST and RAYINVR (*Zelt and Smith*, 1992; *Zelt and Forsyth*, 1994; *Zelt and Barton*, 1998). The former program

inverts first-arrival travel times only by ray tracing through a model with a uniform-velocity mesh. The latter program inverts both first and secondary arrival travel times by ray-tracing through a layered model defined at irregular, discrete depth and velocity nodes. RAYINVR input velocity models can be converted into FAST format velocity models to enable a rapid exploration of potential starting models.

Our RAYINVR model has seven layers: water, sediments, upper crust, middle crust, lower crust, sub-crustal body and mantle. The three crustal layers were included to enable sufficient vertical velocity gradient variation across the entire model to fit the data, but care was taken not to introduce strong velocity contrasts across them as no intra-crustal reflections were observed. The water layer properties were taken from the echo sounder and velocimeter probe measurements and were held fixed throughout the modelling. The initial sediment layer in the deep water part of the model was constructed from picks of the two-way-time to top basement and semblance velocities from reflection line 9. We estimate that the sensitivity of the move-out on the 2.4 km streamer data resolved the semblance velocity to within ± 0.025 km/s throughout the <1km thick sediment column (*Sansom*, 2006). On the plateau, the initial sediment layer was constructed from picks to top basement from commercial reflection profiles (Fig.2, P. Joseph, pers. comm.).

Owing to the relatively small size of the Seychelles microcontinent, recording turning waves from its lower crust presents some difficulties. We overcame this by supplementing the wide-angle data with landstation receiver functions and a historical east-west controlled source refraction line (profile 5210, Fig.4). The controlled source line, which crosses our transect 30 km south of the most southerly landstation on Mahé, (Fig.2) is un-reversed but was collected with tethered sonobuoys (*Davies and Francis*, 1964). The profile was originally interpreted with a line-intercept graphical method so we re-modelled the original first-arrival travel time picks using ray-tracing. This work showed that the 5210 line provided good control on the seismic velocities down to a depth of 20 km from turning waves (Pg), but the structure of the lower crustal layer is determined by mantle refraction Pn alone and hence there

234 is a trade-off between the velocity and thickness of this deepest crustal layer, and there is no
235 information on the details of the lower crustal structure (Fig.4b). Overall the 5210 wide-angle model
236 agrees well with the receiver function-derived profiles, and shows the Seychelles plateau to have a
237 typical continental velocity profile (*Christensen and Mooney*, 1995), with relatively high upper crustal
238 velocities consistent with the exposure of granite on the Islands. The Mahé and Praslin Island receiver
239 functions also showed the base of the crust to have a stepped seismic velocity structure.
240
241 Once the water, sediment, and initial plateau structure had been defined, the first arrival picks were
242 inverted with a range of minimum-structure, geologically reasonable starting models with FAST. This
243 provided a rapid means of determining a suitable starting model for the main modelling phase. The
244 final model was then developed using RAYINVR, with a top-downward approach, and a combination
245 of forward modelling and inversion until the normalised travel-time misfit (χ^2) for the entire dataset fell
246 to 1, and for each individual phase fell below 3 (Table 1). Throughout the travel-time inversion the
247 velocity structure was checked for consistency against the co-incident gravity, seismic reflection and
248 magnetic profile (Fig.3, *Collier et al.*, 2008). For the gravity comparison, a two-dimensional model
249 consisting of homogeneous density blocks was generated directly from the seismic velocity model. The
250 shapes of the density blocks were not dictated by the velocity model layers but were computed from
251 velocity contours chosen to characterise the lateral and vertical variation across the model. The
252 predicted free-air gravity anomaly was then calculated using the two-dimensional line integral
253 algorithm of *Talwani et al.*, (1959). A cross-over error analysis of the gravity data collected in 2003
254 with other historical data from the region showed the likely error in the observed gravity to be ±5mGal.
255 The fit to the gravity was therefore deemed acceptable if it matched to within this uncertainty.
256
257 The resolution of the final velocity model was estimated using the method described in *Zelt and*
258 *Smith* (1992) that quantifies the relative ray coverage at model nodes. A measure of the uncertainty in
259 the final model was gained by perturbing the velocity and depth nodes and re-computing the

normalised travel-time misfit (χ^2). Changes were made to one layer at a time by adding or subtracting a fixed amount to either all the lower velocity or all the lower depth nodes. Once a complete set of perturbations had been made the results were plotted to ensure that the inverted model did indeed represent a minimum solution. The perturbed model χ^2 values were then compared to that of the final model using an F test, and errors assigned to the layer depths and velocities based on the models that were statistically different at the 95% confidence level.

5 Crustal structure

Selected wide-angle record sections and ray diagrams are shown in Fig.5, and the final velocity model in Fig.6. The model shows three distinct provinces: oceanic crust (model x=50-255 km), characterized by thin crust and moderate crustal velocities (4.5-7.2 km/s); transitional crust (model x=255-320 km), characterized by thickening crust and relatively high crustal velocities (5.0-7.3 km/s); and continental crust (model x=255-460 km), characterized by thick crust and relatively low crustal velocities (5.5-6.8 km/s). The overall χ^2 fit of the model to 2272 travel time picks is 0.89, and the rms misfit just 50 ms (Table 1). The phases that are least well matched are the sediment turning ray (Ps), a deep sub-crustal turning ray (Pu) and a deep reflection (PbP), all of which have relatively few total picks and the largest average pick uncertainties. All other phases have a χ^2 of less than 1.4.

The velocity structure of the oceanic crust is notably uniform throughout the length of the profile. The magnetic modelling showed that its age ranges between 63.1 and 60 Ma (Fig.3c, *Collier et al.*, 2008). This part of the seismic model is particularly well-resolved, with clear first arrival crustal turning waves (Pg), post-critical reflection from the Moho (PmP) and mantle refracted arrival (Pn) picks on each of the 8-km spaced seabed instruments (Fig.5a-c). Note that the apparent low model resolution of the sediment layer (Fig.6b) is due to it having a close velocity and depth node spacing defined from the co-incident multichannel data (constraints not included in the RAYINVR model resolution calculation). No sediment turning rays (Ps) were identified on the seabed receivers from this

part of the model and the wide-angle reflection from the basement (PcP) could only be recognised with confidence on about 25% of the instruments. The least well resolved crustal layer is the upper crust, as the first crustal rays to emerge from the direct wave turn just below the top basement. The resolution of all other parts of the model in this region is above the acceptable threshold of 0.5 (*Zelt*, 1999).

The multichannel data show the sediments to thicken from 0.2 to 1 km from north to south across the oceanic crust part of the model. As a result of this change, all the crustal phases arrive later and Pg emerges from the direct wave with higher phase velocities, and hence turns slightly deeper in the crust on instruments to the south (e.g. compare Fig.5a and 5c). Otherwise the only difference in the record sections from OBS33 to OBS55 are small variations in the travel time curves of Pg which correlate with basement topography. Velocity-depth profiles from three points along the oceanic crust section are show in Fig.6c. The seismic velocities increase from about 4.5 to 7.2 km/s with depth. The uncertainty analysis conducted on the crustal layers showed an error of ±0.1 km/s in these velocities. The upper and middle crustal layers have a high velocity gradient of ca. 1.1 /s, whereas the lower crustal layer (model layer 5) has a much smaller gradient of just 0.1 /s. The seismic velocity structure obtained is typical of mature oceanic crust but it is significantly thinner (*White et al.*, 1992). Whilst the high velocity gradient upper crust has a similar thickness to that observed elsewhere, the lower gradient lower crust is thinner by about 2 km. The total crustal thickness averages just 5.2 ±0.11 km along the entire length of this part of the model. Pn is seen on all the instruments here as a first arrival from about 25 km range, and shows the topmost oceanic mantle to have an average velocity of 8.24 km/s with an uncertainty of just ±0.03 km/s.

South of OBS56, the seismic sections change character, with the maximum range of Pg increasing rapidly from 40 to more than 100 km, and both the mantle refraction (Pn) and Moho reflection (PmP), that are widely seen on instruments to the north, disappear. OBH57 is a good illustration of this change, with markedly different –north and –south record sections (Fig.5d). The change in the seismic records

corresponds to the position of the outer seaward-dipping reflectors (SDRs) that are imaged on both the co-incident reflection profile (Fig.3a) and on five of the six other parallel, normal incidence, seismic profiles (Fig.2). Work at other margins has shown that the outer SDRs usually coincide with the continent-ocean transition (*Planke et al.*, 2000). This correlation appears to hold at the Seychelles margin also, and is consistent with our magnetic modelling which showed that a 200 nT positive anomaly could be best explained by the relatively abrupt juxtaposition of non-magnetic continental crust and oceanic crust at this point (Fig.3c, *Collier et al.*, 2008). On several of the seismic profiles there is a clear basement high between the outer and inner SDRs. Similar features at other margins are usually referred to as the *outer high* and interpreted as due to the build up of hyaloclastic flows during explosive shallow water volcanism prior to the establishment of full seafloor spreading (*Planke et al.*, 2000). Inner SDRs are usually interpreted as subaerial flows. This interpretation is supported here by geochemical results from a seamount that lies within the mapped inner SDRs (immediately west of line 12 and south of line 11 at 56^0 12'E, 3^0 34'S, water depth 3400 m, Fig.2). This seamount, which we interpret as a likely feeder to the surrounding SDRs, has a rare earth element pattern which is consistent with subaerial eruption (*Collier et al.*, 2008). On the basis of the seismic and magnetic analysis we therefore place the ocean-continent boundary at model x=255 km, and refer to the model south of this point as the transition zone.

The Pg first arrival times in the transition zone are strongly influenced by the rapidly shallowing seafloor that prevents the direct interpretation of their phase velocities. The travel time inversion however shows that the velocities of the uppermost crust increase to above 5 km/s and the lowermost crust increase slightly to ca 7.3 km/s in this region (Fig.6c). There appears to be a small velocity inversion at about 5 km below top basement. We interpret this velocity structure as due to the presence of the basaltic flows that form the SDRs and basaltic intrusions within the upper continental crust here. The semblance velocities within the overlying sediments also increase to around 3.5 km/s in this region, and there are several particularly strong reflectors in the lower section that we interpret as

basaltic sills. The largest-offset wide-angle arrivals recorded in this region (Pu Fig.5d,5f and 5g) indicate a seismic velocity of 7.6-7.8 km/s, significantly higher than expected for lower continental crust and significantly lower than the 8.24 km/s mantle velocity detected to the north. The most likely interpretation of this material, given its seismic properties and location is that it is mafic material intruded into and underplating the thinned lower continental crust. We model this material as a separate layer, which for ease of reference we have named *underplate*.

South of OBS60, the record sections once again show wide-angle reflections from the lower crust (Fig.5e,5f). Some of the record sections showed two wide-angle reflections, both with similar phase velocities but with a ~0.75s difference in reduced travel time (Fig.5e). Examination of the horizontal geophone components and forward ray tracing showed neither to be converted shear-waves or multiples. We model these events as wide-angle reflections from the top (PtP) and bottom (PbP) of the intruded and underplated material detected by turning event Pu. Assuming the layer velocity to be between 7.6 and 7.8 km/s as indicated by Pu above 15 km depth, the underplate layer needs to be ~4 km thick to explain the observed reflection time difference between PtP and PbP. Further support for the extension of this underplate layer southward beneath the plateau comes from the Seychelles Island receiver functions. Despite the underplate being a somewhat subtle seismic feature (being relatively thin and with an intermediate seismic velocity between lower continental crust and mantle) its presence was detected beneath Praslin (station 10, 10 km thick) and Mahé (station 04, 1 km thick, Fig.4). Note that we do not think it significant that the underplate layer was not detected beneath Denis Island (station 19) as this receiver function had the poorest quality of those obtained and it also failed to resolve upper crustal structure seen on the other two stations.

The offset and reduced time of PtP and PbP varies markedly across adjacent receivers indicating a rapid change in crustal thickness. The reflection travel times were reasonably well-matched by an approximately linear interface dipping at 24^0 between model x=270 and 320 km. Fig.6b shows the

modeled PtP and PbP ray coverage and bounce points. The lack of deep turning rays resulted in the underplate layer being the least-well resolved feature in the model, with a velocity uncertainty of +0.3/-0.35 km/s and thickness uncertainty of +0.7/-0.5 km. The overall shape of the crust however was independently supported by the need to match a prominent 120 mGal positive free air gravity anomaly on the outer Seychelles shelf (Fig.7). Systematic perturbations of the gravity model showed a tolerance of ±3 km in the depth of the lower continental crust layer (density 3.04 g/cm^3). The predicted gravity is not sensitive to the underplate layer itself (density 3.10 g/cm^3), for example removing it entirely changed the predicted gravity by less 5 mGal (the observational uncertainty). As a further external constraint on the shape of the lower crust, the receiver function recorded at Denis Island (x=330 km) showed the crust to be 30 km thick, which is consistent with the PtP reflection seen on the most southerly OBH (Fig.5f). These observations indicate that the lateral distance from the ocean-continent boundary to full-thickness continental crust is just 65 km.

On the Seychelles plateau itself, the wide-angle data further define the upper crustal structure, and show several 1-2 km thick, small sedimentary basins directly overlying > 5.5 km/s basement. The velocity below top basement increases with a gentle gradient of just 0.05/s with depth.

6 Conjugate margin structure

The conjugate Seychelles-Laxmi Ridge margin velocity models are shown together in Fig.8. The two profiles match well, and share a number of common features despite showing overall asymmetry, with the wide, complex Laxmi Ridge margin strongly contrasting with the much simpler and narrower Seychelles margin. Note that the 940 m vertical offset in the depth to basement on the northern margin can be entirely explained by an isostatic response to the load from the thick layer of Indus Fan sediment. We interpret the Laxmi Ridge itself as heavily intruded, thinned continental crust based on its seismic structure and magnetic properties (*Minshull et al.*, 2008; *Collier et al.*, 2008). A set of seaward-dipping reflectors of comparable dimensions to those seen on the Seychelles side are imaged on its southern margin (*Collier et al.*, 2008). Seaward of these SDRs, there is 5 km thick oceanic crust of

chron 27r, which matches the age of that determined on the Seychelles side. The small (200 m) difference from the mean Seychelles oceanic crustal thickness is probably due to limitations of the velocity model in the north, where the velocity gradient at the top of the oceanic crust is poorly constrained because turning arrivals from this layer are obscured by earlier sedimentary arrivals. To the north of the Laxmi Ridge, the Gop Rift is interpreted as a failed rift underlain by oceanic crust. This interpretation is based on its seismic structure, presence of SDRs on its northern margin, and occurrence of strong magnetic anomalies symmetrically about a prominent basement ridge in the centre of the rift that we interpret as an extinct spreading axis. Given that the Carlsberg Ridge has generated an unbroken set of magnetic anomalies from 27r to the present day, the Gop Rift must have opened before the Seychelles rifted. Unfortunately, the Gop Rift is narrow and the magnetic anomaly sequence is too short to identify it uniquely (*Collier et al.*, 2008). The mean thickness of the oceanic crust in the Gop Rift is 9 km, significantly thicker than that formed by the young Carlsberg ridge between the Laxmi Ridge and Seychelles. At the northern end of the profile, the crust is interpreted as continental crust marking the tapered edge of the Indian continental crust (*Malod et al.*, 1997). The crust here is underlain by a high velocity sub-crustal body which, like that beneath the Seychelles, is constrained by wide-angle reflections from its top and base. The body, which due to the imaging geometry is better resolved than in the Seychelles model, reaches a maximum thickness of ~12 km and has a velocity of 7.4 km/s. A second region with similar properties and hence also interpreted as underplate is imaged beneath the Laxmi Ridge itself, where it is constrained by both wide-angle reflections and turning waves. The robust detection of these underplate bodies beneath the northern conjugate margin lends support to our interpretation of PtP and PbP on the Seychelles side. The geometry of the underplate bodies suggest that they were formed when the Gop Rift opened. If they had formed during the Seychelles-Laxmi Ridge rift event they would be expected to be continuous across the Gop Rift (*Minshull et al.*, 2008). Instead normal mantle velocities below normal lower oceanic crustal velocities were found in the Gop Rift. Significant underplating is also more consistent with the generation of

thickened oceanic crust within the Gop Rift than the thin oceanic crust at the north Seychelles/south Laxmi Ridge margins.

7 Discussion

7.1 Comparison with other margins

7.1.1 Sub-aerial volcanism

Some of the first seaward-dipping reflectors (SDRs) were identified along the Indian Margin (*Hinz*, 1981) but since this early discovery the presence of extensive SDRs there has not been confirmed (*Gaedicke et al.*, 2002; *Krishna et al.*, 2006; *Minshull et al.*, 2008). At the north Seychelles margin although SDRs were imaged on most of our multichannel seismic lines (see Fig.2 for their mapped distribution), they are not well-expressed. Two sets of SDRs are present, an outer (oceanward) and inner (landward), the latter set being more widely and robustly imaged in our dataset. Each set of SDRs is imaged for about 10 km along track with individual reflectors being traced laterally for up to 6 km (Fig.3a, Fig.9a). The best-imaged set of reflectors is on line 13, where they reach a total thickness of 0.75 s TWT. In comparison, at the Edoras Bank margin of the North Atlantic, which at ca.1100 km from the Iceland plume should be comparable with the Seychelles margin, the SDRs extend laterally for 70 km and are 2 s TWT thick (Fig.9, *Barton and White*, 1997). Although the sediments are thicker at the Seychelles than at the Edoras margin, given the widespread imaging of Moho beneath the SDRs in our data, we do not consider that this difference is a result of poor seismic energy penetration. Whilst care needs to be taken when drawing conclusions from SDRs as it has been shown that seaward-dipping lava formations may exist without having a seismic expression (*Eldholm et al.*, 1986; *Planke and Eldholm*, 1994; *Planke et al.*, 2000), the poor development of SDRs at the Seychelles margin is consistent with modest subaerial/shallow marine volcanism that would be expected to precede the generation of 5.2 km thick oceanic crust.

439 It is also significant that we found no evidence for a thick flood basalt sequence on top of the
440 northern Seychelles plateau. In western India the upper continental crust is characterised by a velocity
441 inversion with an up to 3 km layer of 4.8-5.1 km/s basalts overlying 1-2 km of Mesozoic sediments
442 with velocities of 3.1-3.2 km/s (*Reddy*, 2005). Whilst we have evidence for a small velocity inversion
443 on the slope, there is no evidence for one on the plateau itself. Instead, on the plateau, a number of
444 isolated, 1-2 km thick, small sedimentary basins with velocities of 2.5-3.5 km/s directly overly > 5.5
445 km/s basement. The upper continental crustal structure is particularly well-resolved in our model, and
446 so a thick basaltic layer is certainly missing. This observation is important as the entire northern
447 Mascarene Plateau from the Saya de Malha Bank up to and including most or all of the Seychelles
448 plateau (the region between the labels "MP" and "SP" in Fig.1c, an area of 2.5 x10^5 km^2) has been
449 previously included as part of the Deccan province by both *White and McKenzie* (1989) and *Coffin and*
450 *Eldholm* (1994). We consider it unlikely that a significant part of the northern Mascarene Ridge south
451 of the Seychelles continental block could have been formed during the main phase of Deccan activity
452 without significantly more offshore magmatism being produced during continental break-up. The
453 spatial extent of the Deccan flood basalt province is therefore smaller than previously thought.

454 ***7.1.2 Initial oceanic crustal and margin width***

455 In order to investigate the significance of the initial oceanic crustal thickness generated at the
456 Seychelles margin we made a compilation of observations at other margins (Table2). We restricted our
457 analysis to studies in which the crustal structure was constrained by modern wide-angle seismic
458 methods, except in the South Atlantic where in order to achieve a reasonable geographical coverage we
459 included one study that relied on gravity modelling of multi-channel seismic data (*Mohriak et al.*,
460 1998) and one that relied on sonobuoys (*Chang et al.*, 1992). For areas such as offshore Norway, where
461 there were many suitable surveys, only one representative survey per region was chosen. We included
462 the Gulf of California margins in the compilation but we note that these three profiles show unusually
463 rapid along strike changes in structure which have been attributed to the local setting (*Lizarralde et al.*,
464 2007). The geographic distribution of our selected profiles is shown in Fig.10. The thickness of earliest

oceanic crust was measured from the original published velocity models at the point immediately seaward of the outer SDRs in the case of volcanic margins or immediately seaward of serpentinised mantle in the case of non-volcanic margins. For profiles where neither of these features was present, the thickness was measured on the oldest unequivocal oceanic crust as indicated by the seismic velocity structure, reflective nature of the top basement and magnetics. Care was taken to ensure a consistent a set of measurement points as possible, which required some re-interpretation of crustal type compared to that given by the original authors in a few cases. In the case of the North and South Atlantic profiles, we then computed their distance from the Iceland and Tristan da Cunha hotspots respectively at the time of continental break-up inferred from the positions of their associated aseismic ridges (Fig.10). We chose to exclude the non-volcanic Labrador Sea margins (*Chian and Louden*, 1994; *Chian et al.*, 1995) from the North Atlantic province as it is commonly argued that they rifted before the Iceland hotspot initiated (*White and McKenzie*, 1989). However we note that the age of the oldest oceanic crust here is disputed, and other authors consider that the margins formed within ca 700 km of the starting Iceland plume (*Nielsen et al.*, 2002).

Our compilation showed that the 5.2 km thick oceanic crust formed at the north Seychelles margin is indisputably thin. Indeed, somewhat surprisingly given the tectonic setting of the Seychelles margin, the oceanic crust here is even thinner than many of the non-volcanic margins listed in Table 2, that have an average of 5.8 ± 1.0 km (excluding the Moroccan margin where oceanic crust may have been thickened by later volcanism, *Contrucci et al.*, 2004a). Next, we plotted selected margin parameters in order to test relationships predicted by current rift-magmatism models. The first relationship we investigated was oceanic crustal thickness versus distance from hotspot centre (Fig.11a). The North Atlantic margins, which have been particularly well studied with many high-quality profiles, show a clear, approximately linear reduction in the thickness of the earliest-formed oceanic crust with distance from the centre of the Greenland-Iceland-Faeroe Ridge. This pattern has been previously interpreted by *Barton and White* (1997) as due to a reduction in the mantle thermal anomaly with distance away from

491 the Iceland plume at the time of rifting. At distances away from the Iceland plume similar to those of
492 our Seychelles profile from the Deccan hotspot, the oceanic crustal thickness found along the North
493 Atlantic margins is more than twice as thick. The relationship between distance from hotspot centre and
494 thickness of the first formed oceanic crust in the South Atlantic is less clear, perhaps in part due to the
495 smaller number and poorer quality of observations. However here too there appears to be an
496 approximately linear relationship, and the oceanic crust at similar distances to the Seychelles study area
497 is one and a half times thicker.
498
499 The second relationship we investigated was oceanic crustal thickness versus margin width
500 (Fig.11b). We define margin width as the distance from the point at which we measured the initial
501 oceanic crustal thickness to the position of full thickness continental crust (itself defined as a thickness
502 of more than 25 km unless the crustal model suggested a smaller value was acceptable). Whilst there is
503 considerable scatter in the data, our new compilation confirms the tendency for the thickness of the
504 first-formed oceanic crust to reduce with increasing margin width, as previously noted by the authors of
505 the small-scale convection models (*Mutter et al.*, 1988). However, as can be seen from the compilation
506 the Seychelles margin is relatively narrow and therefore these models would predict it to have
507 thickened oceanic crust, although possibly active convection was damped by the wide Laxmi conjugate
508 margin. In addition to crustal thickness, the seismic velocity of the oceanic crust formed along
509 continental margins may also be diagnostic of the rift dynamics (*Kelemen and Holbrook*, 1995;
510 *Holbrook et al.*, 2001). According to these workers, active convection is expected to generate oceanic
511 crust with a lower seismic velocity than that generated by passive melting under elevated mantle
512 temperature because melting occurs shallower and so produces melts poorer in MgO and richer in SiO_2.
513 Following the approach detailed in *Holbrook et al.*, (2001), we calculate a mean oceanic crustal
514 velocity of 6.93 ± 0.02 km/s for the north Seychelles margin. According to their model (Fig.11c), this
515 seismic velocity coupled with a mean thickness of 5.2 ±0.1 km, indicates that the crust formed by
516 passive upwelling only (i.e. no small-scale convection) with a mantle potential temperature of 1275^0C

517 (i.e. slightly cooler than "normal" 1300^{0}C mantle). Results for the distal Greenland margins (dots
518 labelled 4b and 4c, Fig.11c) also indicate a lack of active upwelling but the predicted mantle
519 temperatures are 100^{0}C hotter. We note that the fast-spreading (65 mm/a) Seychelles oceanic crust has
520 very similar properties to the fast-spreading East Pacific Rise at 17^{0}S (diamond labelled epr, Fig.11c).
521 Based on this result we will not discuss active upwelling models further.

522 ## *7.2 Factors influencing magmatism during continental break-up*

523 Our observations at the Seychelles margin are at odds with the predictions of the plume head
524 model of melt generation during continental break-up. In this model the voluminous magmatism
525 observed at volcanic continental margins is due to the transient high temperatures and flow rates
526 generated as a new plume impacts the base of the lithosphere (*White and McKenzie*, 1989; *White*,
527 1992b). Several workers have noted that the 2000-2500 km extent of the volcanic margins that border
528 the north Atlantic is comparable with the theoretical predictions of a diameter of a flattened circular
529 plume head, and cited this observation as support for this model (*Campbell*, 2007). If this scenario is
530 correct, then we would need to invoke a smaller/colder plume head in the Deccan case to match our
531 new seismic observations. However, we note that the volume of the onshore Deccan is estimated to be
532 very similar to that of both the onshore North Atlantic Tertiary Volcanic and the South American
533 Parana provinces (extrusive components 1.5 x10^6 km^3, 1.8 x10^6 km^3 and >1.5 x10^6 km^3 respectively,
534 *Coffin and Eldholm*, 1994; *White and McKenzie*, 1995), and so it seems more reasonable to infer that
535 they originated from mantle plumes of similar sizes and temperatures. Indeed, theoretical work shows
536 that mantle plume size and temperature is largely dictated by the height of ascent, so if the Iceland,
537 Tristan de Cunha and Reunion plumes all formed from the same depth (be it the base of the mantle or
538 base of the upper mantle) they should have had similar properties (*Campbell*, 2007). We conclude that
539 the symmetrical flattened plume head model is not compatible with our observations at the north
540 Seychelles margin.
541

Several workers have previously emphasised that the lateral flow of plume material beneath the lithosphere may not be a simple radial process, such that the distribution of hot material beneath a region experiencing plume-impact is case-specific. If this is correct then it would not be appropriate to directly compare the extent of volcanic rifted margins to the dimensions of the flattened, circular plume head (*Sleep*, 1997). Lateral flow could also be important for non-plume sources for the flood basalt generation, such as edge-driven convection, where a central zone of upwelling mantle flows laterally beneath the surrounding lithosphere. In the plume case, the variation in the spatial distribution of the thermal anomaly might be exacerbated if, rather than having an axisymmetric ("mushroom head") geometry, the arriving plume head had a more complicated shape, such as an initial three-armed form, as has been predicted in some numerical models (e.g. *Houseman*, 1990) and it does not have a long incubation period beneath the lithosphere in which to thermally equilibrate prior to rifting. Hence it may not be appropriate to expect all margins formed at similar lateral distances from the centre of a similarly sized plume to display common magmatic characteristics. *Nielsen et al.,* (2002) applied this idea to explain the formation of the non-volcanic margins of the Labrador Sea (which they believe formed within the North Atlantic province) as being due to the flow of Iceland plume material being blocked by the thick Greenland craton. This idea, however, is not so readily applied in the Seychelles case, as it could be argued that the plume material would be expected to have flowed upslope from the Indian craton towards the Seychelles, given that the lithosphere here was probably already thinned when Greater India split from Madagascar ca 20 Ma earlier. Perhaps when the Gop Rift opened it exhausted the hot asthenospheric layer bought by the plume. Alternatively, in the Iceland case hot material could have been preferentially fed into the North Atlantic margins because the developing rift intersected the central stem of the new plume. In the case of the Seychelles, the margin is offset from the Deccan centre and the "plume-tail" Chagos-Laccadive ridge is not orthogonal to the continental margins (Fig.1a). It has also been suggested that the South Atlantic margins did not intersect the plume axis either (*Peate et al.*, 1990; *Harry and Sawyer*, 1992), and so perhaps this is also the explanation for the lower degree of magmatism observed along these margins compared to those in the North Atlantic.

An intriguing alternative possibility is that the difference in the structure of the Seychelles and distal Atlantic margins is related to differences in efficiency of melt extraction at varying plate divergence rates. In order to investigate this idea, we plotted the thickness of the initial oceanic crust against initial seafloor spreading rate for each of our compiled continental margins together with other measurements of oceanic crust thickness made away from continental margins (Fig.11d). In this diagram, the relatively high initial seafloor spreading rate of the Seychelles margin is highlighted. It may be significant that the Eastern Somali Basin/Arabian Sea opened more than three times faster than the North Atlantic and twice as fast as the South Atlantic. Current pure-passive melting models do not predict any change in oceanic crustal thickness with spreading rate, except at ultra-slow seafloor spreading rates (*Bown and White*, 1994). Rather, as the spreading rate increases the flux of mantle across the solidus increases and a constant thickness oceanic crust results (*Niu and Hekinian*, 1997). However such models assume 100% melt extraction, and perhaps as the width of the melting region increases this is not achieved in reality. In support of this idea we note that the current catalogue of steady-state "normal" oceanic thickness (those measured away from continental margins and marked with inverted triangles in Fig.11d) trend towards < 6km crustal thickness for spreading rates above 55 mm/yr. It is possible that even if there was a modest thermal anomaly at the Seychelles margin at the time of rifting, due to the rapid plate divergence all the melt generated from the wide melting zone could not be extracted and thickened oceanic crust and other features associated with excess magmatism such as extensive SDRs were not produced.

8 Conclusions

The crustal structure determined at the north Seychelles margin (and its conjugate) is characterised by thin oceanic crust, weak expression of seaward-dipping reflectors, and an earlier, pre-rift underplate of uncertain age. The plateau itself is underlain by 32 km thick continental crust, without any seismic evidence for a thick layer of extruded basalt on its surface. A significant inference from our work is

therefore that the two most commonly cited estimates of the spatial extent of the Deccan-onshore-offshore province – those of *White and McKenzie* (1989) and *Coffin and Eldholm* (1994) - are too large. The Deccan mantle source cannot have had the ~2500 km diameter, axisymmetric shape commonly depicted in the literature.

The pattern of magmatism observed at the north Seychelles continental margin is very different to that observed at previously studied margins that rifted shortly after the eruption of a near-by onshore flood-basalt province. In particular the oceanic crust north of the Seychelles is just 5.2 ± 0.1 km thick, and this remained more or less constant for the first 3 Ma of seafloor spreading. In contrast equivalent margins in the North and South Atlantic have initial oceanic crust that is two and one-and-a-half times thicker, respectively, with normal thickness oceanic crust not being produced until 5-10 Ma after rifting. We conclude that our current understanding of the factors influencing the degree of magmatism during continental break-up is incomplete. We speculate that either the lateral flow of hot material beneath the region was hampered in the Seychelles case, perhaps as the rifted margins did not intersect the centre of the Deccan mantle source, or there was incomplete melt extraction from the wide melting region that formed between the rapidly diverging plates. If the latter is correct then the rate of plate separation, as indicated by the initial seafloor spreading rate, is more important in controlling the volume of magmatism generated during continental rifting than has been previously recognised.

9 Acknowledgements

We thank everyone who sailed on RRS Charles Darwin cruises CD134b and CD144 and the many people who helped with the installation and running of the land stations. Patrick Joseph of the Seychelles National Oil Company provided access to commercial seismic and magnetic data from the plateau, Bob Fisher of Scripps Institution of Oceanography provided an unpublished, hand contoured bathymetric chart of the Seychelles region, Ed Stephens of St. Andrews University provided magnetic measurements for a variety of Seychelles rock samples and Bob White of Cambridge University

620 provided access to the passive melting code. Fiona Hall, Mark Vardy and Mikhail Evain helped with
621 the data analysis. The seismic data were processed using ProMax software available via a software
622 grant to Imperial College London from Landmark Graphics. This work was funded by the UK Natural
623 Environment Research Council grants NER/A/S/2000/01332, NER/A/S/2000/01390 and
624 NER/A/S/2000/01391 and access to the OBS was via European Union Human Capacity grant HPRI-
625 CT-1999-00037. We thank Douglas Toomey, Keith Louden and Daniel Lizarralde for their
626 constructive reviews.
627

10 References

Anderson, D.L., (1994), The Sublithospheric Mantle as the Source of Continental Flood Basalts - the Case against the Continental Lithosphere and Plume Head Reservoirs, *Earth and Planetary Science Letters*, *123* (1-4), 269-280.

Armitage, J.J., T.J. Henstock, T.A. Minshull, and J.R. Hopper, (2008), Modelling the composition of melts formed during continental breakup of the Southeast Greenland margin, *Earth and Planetary Science Letters*, *269* (1-2), 248-258.

Barton, A.J., and R.S. White, (1997), Crustal structure of Edoras Bank continental margin and mantle thermal anomalies beneath the North Atlantic, *Journal of Geophysical Research-Solid Earth*, *102* (B2), 3109-3129.

Bauer, K., S. Neben, B. Schreckenberger, R. Emmermann, K. Hinz, N. Fechner, K. Gohl, A. Schulze, R.B. Trumbull, and K. Weber, (2000), Deep structure of the Namibia continental margin as derived from integrated geophysical studies, *Journal of Geophysical Research-Solid Earth*, *105* (B11), 25829-25853.

Bown, J.W., and R.S. White, (1994), Variation with Spreading Rate of Oceanic Crustal Thickness and Geochemistry, *Earth and Planetary Science Letters*, *121* (3-4), 435-449.

Bullock, A.D., and T.A. Minshull, (2005), From continental extension to seafloor spreading: crustal structure of the Goban Spur rifted margin, southwest of the UK, *Geophysical Journal International*, *163* (2), 527-546.

Campbell, I.H., (2007), Testing the plume theory, *Chemical Geology*, *241* (3-4), 153-176.

Chang, H.K., R.O. Kowsmann, A.M.F. Figueiredo, and A.A. Bender, (1992), Tectonics and stratigraphy of the East Brazil rift system - an overview, *Tectonophysics*, *213* (1-2), 97-138.

Chian, D., I.D. Reid, and H.R. Jackson, (2001), Crustal structure beneath Orphan Basin and implications for nonvolcanic continental rifting, *Journal of Geophysical Research-Solid Earth*, *106* (B6), 10923-10940.

Chian, D.P., and K.E. Louden, (1994), The continent-ocean crustal transition across the southwest Greenland margin, *Journal of Geophysical Research-Solid Earth*, *99* (B5), 9117-9135.

Chian, D.P., K.E. Louden, and I. Reid, (1995), Crustal structure of the Labrador Sea conjugate margin and implications for the formation of nonvolcanic continental margins, *Journal of Geophysical Research-Solid Earth*, *100* (B12), 24239-24253.

Christensen, N.I., and W.D. Mooney, (1995), Seismic velocity structure and composition of the continental crust: a global review, *Journal of Geophysical Research-Solid Earth*, *100* (B7), 9761-9788.

Coffin, M.F., and O. Eldholm, (1994), Large Igneous Provinces - crustal structure, dimensions, and external consequences, *Reviews of Geophysics*, *32* (1), 1-36.

Collier, J.S., V. Sansom, O. Ishizuka, R.N. Taylor, T.A. Minshull, and R.B. Whitmarsh, (2008), Age of Seychelles-India break-up, *Earth and Planetary Science Letters*, *272*, 264-277.

Contrucci, I., F. Klingelhofer, J. Perrot, R. Bartolome, M.A. Gutscher, M. Sahabi, J. Malod, and J.P. Rehault, (2004a), The crustal structure of the NW Moroccan continental margin from wide-angle and reflection seismic data, *Geophysical Journal International*, *159* (1), 117-128.

Contrucci, I., L. Matias, M. Moulin, L. Geli, F. Klingelhofer, H. Nouze, D. Aslanian, J.L. Olivet, J.P. Rehault, and J.C. Sibuet, (2004b), Deep structure of the West African continental margin (Congo, Zaire, Angola), between 5 degrees S and 8 degrees S, from reflection/refraction seismics and gravity data, *Geophysical Journal International*, *158* (2), 529-553.

Courtillot, V.E., and P.R. Renne, (2003), On the ages of flood basalt events, *Comptes Rendus Geoscience*, *335* (1), 113-140.

Davies, D., and T.J.G. Francis, (1964), The crustal structure of the Seychelles Bank, *Deep-Sea Research*, *11*, 921-927.

Dean, S.M., T.A. Minshull, R.B. Whitmarsh, and K.E. Louden, (2000), Deep structure of the ocean-continent transition in the southern Iberia Abyssal Plain from seismic refraction profiles: The IAM-9 transect at 40 degrees 20 ' N, *Journal of Geophysical Research-Solid Earth*, *105* (B3), 5859-5885.

Duncan, R.A., J. Backman, and L.C. Peterson, (1990), *Proceedings of the Ocean Drilling Program, Scientific results, 115*, Ocean Drilling Program, College Station, TX.

Duncan, R.A., and R.B. Hargraves, (1990), $^{40}Ar/^{39}Ar$ geochronology of basement rocks from the Mascarene Plateau, the Chagos Bank and the Maldives Ridge., in *Proc. ODP, Scientific Results, Vol 115*, edited by R.A. Duncan, J. Backman, and L.C. Peterson, pp. 43-51, Ocean Drilling Program, College Station, TX.

Eldholm, O., J. Thiede, E. Taylor, K. Bjorklund, U. Bleil, P. Cielsielski, A. Desprairies, D. Donally, C. Froget, R. Goll, R. Henrich, E. Jansen, L. Krissek, K.A. Kvenvolden, A. LeHuray, D. Love, P. Lysne, T. McDonald, P. Mudie, L. Osterman, L.M. Parson, J. Phillips, A. Pittenger, G. Qvale, G. Schoenhartin, and L. Viereck, (1986), Dipping reflectors in the Norwegian Sea; ODP Leg 104 drilling results, *Journal of the Geological Society*, *143* (6), 911-912.

Fernandez-Viejo, G., J. Gallart, J.A. Pulgar, J. Gallastegui, J.J. Danobeitia, and D. Cordoba, (1998), Crustal transition between continental and oceanic domains along the North Iberian margin from wide angle seismic and gravity data, *Geophysical Research Letters*, *25* (23), 4249-4252.

Flueh, E.R., and J. Bialas, (1996), A digital, high data capacity ocean bottom recorder for seismic investigations, *Int. Underwater Systems Design*, *18* (3), 18-20.

Fowler, S.R., R.S. White, G.D. Spence, and G.K. Westbrook, (1989), The Hatton Bank continental-margin .2. Deep-structure from 2-ship expanding spread seismic profiles, *Geophysical Journal-Oxford*, *96* (2), 295-309.

Francis, T.J.G., D. Davies, and M.N. Hill, (1966), Crustal structure between Kenya and the Seychelles, *Philosophical Transactions of the Royal Society of London*, *259* (A), 240-261.

Francis, T.J.G., and G.G. Shor, (1966), Seismic refraction measurements in the Northwest Indian Ocean, *Journal of Geophysical Research*, *71* (2), 427-449.

Franke, D., S. Neben, B. Schreckenberger, A. Schulze, M. Stiller, and C.M. Krawczyk, (2006), Crustal structure across the Colorado Basin, offshore Argentina, *Geophysical Journal International*, *165* (3), 850-864.

Funck, T., J.R. Hopper, H.C. Larsen, K.E. Louden, B.E. Tucholke, and W.S. Holbrook, (2003), Crustal structure of the ocean-continent transition at Flemish Cap: Seismic refraction results, *Journal of Geophysical Research-Solid Earth*, *108* (B11), 2531, doi:10.1029/2003JB002434.

Funck, T., H.R. Jackson, K.E. Louden, S.A. Dehler, and Y. Wu, (2004), Crustal structure of the northern Nova Scotia rifted continental margin (eastern Canada), *Journal of Geophysical Research-Solid Earth*, *109* (B9), B09102, doi:10.1029/2004JB003008.

Gaedicke, C., H.U. Schluter, H.A. Roeser, A. Prexl, B. Schreckenberger, H. Meyer, C. Reichert, P. Clift, and S. Amjad, (2002), Origin of the northern Indus Fan and Murray Ridge, Northern Arabian Sea: interpretation from seismic and magnetic imaging, *Tectonophysics*, *355* (1-4), 127-143.

Gaskell, T.F., M.N. Hill, and J.C. Swallow, (1958), Seismic measurements made by H.M.S. Challenger in the Atlantic, Pacific and Indian Oceans and in the Mediterranean Sea, 1950-53, *Phil. Trans. Roy. Soc. London A*, *251*, 23-83.

Goldschmidt-Rokita, A., K.J.F. Hansch, H.B. Hirschleber, T. Iwasaki, T. Kanazawa, H. Shimamura, and M.A. Sellevoll, (1994), The ocean continent transition along a profile through the Lofoten Basin, northern Norway, *Marine Geophysical Researches*, *16* (3), 201-224.

Gradstein, F.M., J.G. Ogg, and A.G. Smith, (2005), *A Geologic Time Scale 2004*, 610 pp., CUP, Cambridge, UK.

Greenroyd, C.J., C. Peirce, M. Rodger, A.B. Watts, and R.W. Hobbs, (2007), Crustal structure of the French Guiana margin, west equatorial Atlantic, *Geophysical Journal International*, *169* (3), 964-987.

Hammond, J.O.S., J.-M. Kendall, G. Helffrich, J.S. Collier, and G. Rumpker, (submitted), Crust and upper mantle structure beneath the Seychelles: Architecture of a microcontinent, *Geophysical Journal International*.

Hammond, J.O.S., J.-M. Kendall, G. Rumpker, J. Wookey, N. Teanby, P.R. Joseph, T.M. Ryberg, and G. Stuart, (2005), Upper-mantle anisotropy beneath the Seychelles microcontinent, *Journal of Geophysical Research*, *110* (B11).

Harry, D.L., and D.S. Sawyer, (1992), Basaltic Volcanism, Mantle Plumes, and the Mechanics of Rifting - the Parana Flood-Basalt Province of South-America, *Geology*, *20* (3), 207-210.

Helffrich, G., (2006), Extended-time multi-taper frequency domain cross-correlation receiver function estimation, *Bull. Seism. Soc. Am*, *96*, 344-347.

Hinz, K., (1981), A hypothesis on terrestrial catastrophes: Wedges of very thick oceanward dipping layers beneath passive continental margins - their origin and paleoenvironmental significance, *Geologisches Jahrbuch*, *E22*, 3-28.

Holbrook, W.S., H.C. Larsen, J. Korenaga, T. Dahl-Jensen, I.D. Reid, P.B. Kelemen, J.R. Hopper, G.M. Kent, D. Lizarralde, S. Bernstein, and R.S. Detrick, (2001), Mantle thermal structure and active upwelling during continental breakup in the North Atlantic, *Earth and Planetary Science Letters*, *190* (3-4), 251-262.

Holbrook, W.S., G.M. Purdy, R.E. Sheridan, L. Glover, M. Talwani, J. Ewing, and D. Hutchinson, (1994a), Seismic structure of the US mid-Atlantic continental-margin, *Journal of Geophysical Research-Solid Earth*, *99* (B9), 17871-17891.

Holbrook, W.S., E.C. Reiter, G.M. Purdy, D. Sawyer, P.L. Stoffa, J.A. Austin, J. Oh, and J. Makris, (1994b), Deep structure of the United-States Atlantic continental-margin, offshore south-Carolina, from coincident ocean-bottom and multichannel seismic data, *Journal of Geophysical Research-Solid Earth*, *99* (B5), 9155-9178.

Hooper, P.R., (1990), The timing of crustal extension and the eruption of continental flood basalts, *Nature*, *345* (6272), 246-249.

Hopper, J.R., J.C. Mutter, R.L. Larson, C.Z. Mutter, P. Buhl, J.B. Diebold, J. Alsop, D. Falvey, P. Williamson, F. Brassil, and J.M. Lorenzo, (1992), Magmatism and rift margin evolution - evidence from northwest Australia, *Geology*, *20* (9), 853-&.

Houseman, G.A., (1990), The thermal structure of mantle plumes - axisymmetric or triple-junction, *Geophysical Journal International*, *102* (1), 15-24.

Keen, C.E., and R.R. Boutilier, (2000), Interaction of rifting and hot horizontal plume sheets at volcanic margins, *Journal of Geophysical Research-Solid Earth*, *105* (B6), 13375-13387.

Kelemen, P.B., and W.S. Holbrook, (1995), Origin of Thick, High-Velocity Igneous Crust Along the US East-Coast Margin, *Journal of Geophysical Research-Solid Earth*, *100* (B6), 10077-10094.

Krishna, K.S., D.G. Rao, and D. Sar, (2006), Nature of the crust in the Laxmi Basin (14 degrees-20 degrees N), western continental margin of India, *Tectonics*, *25* (1).

Lane, C.I., Rifted margin formation in the northwest Indian ocean: the extensional and magmatic history of the Laxmi Ridge continental margin., PhD Thesis, University of Southampton, 2006.

Langmuir, C.H., E.M. Klein, and T. Plank, (1992) Petrological systematics of mid-ocean ridge basalts: Constraints on melt generation beneath ocean ridges, in *Mantle Flow and Melt Generation at Mid-Ocean Ridges*, *Geophys. Monogr. No. 71*, edited by J.P. Morgan, Blackman, D. K. & Sinton, J. M, pp. 183-280, Am. Geophys. Union, Washington DC.

Langston, C.A., (1979), Structure under Mount Rainier, Washington, inferred from teleseismic body waves, *J. Geophys. Res.*, *84*, 4749-4762.

Lau, K.W.H., K.E. Louden, T. Funck, B.E. Tucholke, W.S. Holbrook, J.R. Hopper, and H.C. Larsen, (2006), Crustal structure across the Grand Banks-Newfoundland Basin continental margin - I. Results from a seismic refraction profile, *Geophysical Journal International*, *167* (1), 127-156.

Lizarralde, D., G.J. Axen, H.E. Brown, J.M. Fletcher, A. Gonzalez-Fernandez, A.J. Harding, W.S. Holbrook, G.M. Kent, P. Paramo, F. Sutherland, and P.J. Umhoefer, (2007), Variation in styles of rifting in the Gulf of California, *Nature*, *448* (7152), 466-469.

Ludwig, W.J., J.E. Nafe, and C.L. Drake, (1970), Seismic refraction, in *The Sea, vol 4, New concepts of seafloor evolution*, edited by A.E. Maxwell, Wiley-Interscience.

Malod, J.A., L. Droz, B.M. Kemal, and P. Patriat, (1997), Early spreading and continental to oceanic basement transition beneath the Indus deep-sea fan: northeastern Arabian Sea, *Marine Geology*, *141* (1-4), 221-235.

McKenzie, D.P., and M. Bickle, (1988), The volume and composition of melt generated by extension of the lithosphere, *J. Petrology*, *29*, 625-679.

Miles, P.R., and W.R. Roest, (1993), Earliest seafloor spreading magnetic anomalies in the north Arabian Sea and the ocean-continent transition, *Geophys. J. Int.*, *15*, 1025-1031.

Minshull, T.A., S.M. Dean, R.S. White, and R.B. Whitmarsh, (2001), Anomalous melt production after continental break-up in the southern Iberia Abyssal Plain, in *Non-Volcanic Rifting of Continental Margins: A Comparison of Evidence from Land and Sea*, edited by R.C.L. Wilson, R.B. Whitmarsh, B. Taylor, and N. Froitzheim, pp. 537-550, The Geological Society of London, London.

Minshull, T.A., C.I. Lane, J.S. Collier, and R.B. Whitmarsh, (2008), Rifting and Magmatism in the Northeastern Arabian Sea, *Nature Geoscience*, *1* (7), 463-467.

Mjelde, R., T. Raum, B. Myhren, H. Shimamura, Y. Murai, T. Takanami, R. Karpuz, and U. Naess, (2005), Continent-ocean transition on the Voring Plateau, NE Atlantic, derived from densely sampled ocean bottom seismometer data, *Journal of Geophysical Research-Solid Earth*, *110* (B5), B05101, doi:10.1029/2004JB003026.

Mjelde, R., M.A. Sellevoll, H. Shimamura, T. Iwasaki, and T. Kanazawa, (1992), A crustal study off Lofoten, N. Norway, by use of 3-component ocean bottom seismographs, *Tectonophysics*, *212* (3-4), 269-288.

Mohriak, W.U., M. Bassetto, and I.S. Vieira, (1998), Crustal architecture and tectonic evolution of the Sergipe-Alagoas and Jacuipe basins, offshore northeastern Brazil, *Tectonophysics*, *288* (1-4), 199-220.

Muller, R.D., M. Sdrolias, C. Gaina, and W.R. Roest, (2008), Age, spreading rates, and spreading asymmetry of the world's ocean crust, *Geochemistry Geophysics Geosystems*, *9*.

Mutter, J.C., W.R. Buck, and C.M. Zehnder, (1988), Convective partial melting .1. A model for the formation of thick basaltic sequences during the initiation of spreading, *Journal of Geophysical Research-Solid Earth*, *93* (B2), 1031-1048.

Mutter, J.C., and R.L. Larson, (1989), Extension of the Exmouth Plateau, offshore northwestern Australia: Deep seismic reflection/refraction evidence for simple and pure shear mechanisms, *Geology*, *17* (1), 15-18.

Mutter, J.C., and C.M. Zehnder, (1988), Deep crustal structure and magmatic processes: the inception of seafloor spreading in the Norwegian-Greenland Sea, in *Early Tertiary Volcanism and the Opening of the NE Atlantic*, edited by A.C. Morton, and L.M. Parson, pp. 35-48, Geological Society of London.

Naini, B.R., and M. Talwani, (1982), Structural framework and the evolutionary history of the continental margin of western India, in *Studies in continental margin geology*, edited by J.S. Watkins, and C.L. Drake, pp. 167-191, Amer. Assoc. Pet. Geol, Tulsa, OK.

Nielsen, T.K., and J.R. Hopper, (2004), From rift to drift: Mantle melting during continental breakup, *Geochemistry Geophysics Geosystems*, *5*.

Nielsen, T.K., H.C. Larsen, and J.R. Hopper, (2002), Contrasting rifted margin styles south of Greenland: implications for mantle plume dynamics, *Earth and Planetary Science Letters*, *200* (3-4), 271-286.

Nissen, S.S., D.E. Hayes, P. Buhl, J. Diebold, B.C. Yao, W.J. Zeng, and Y.Q. Chen, (1995), Deep Penetration Seismic-Soundings across the Northern Margin of the South-China-Sea, *Journal of Geophysical Research-Solid Earth*, *100* (B11), 22407-22433.

Niu, Y.L., and R. Hekinian, (1997), Spreading-rate dependence of the extent of mantle melting beneath ocean ridges, *Nature*, *385* (6614), 326-329.

Norton, I.O., and J.G. Sclater, (1979), A model for the evolution of the Indian Ocean and the breakup of Gondwanaland, *Journal of Geophysical Research*, *84* (B12), 6803-6830.

Olafsson, I., E. Sundvor, O. Eldholm, and K. Grue, (1992), More margin - crustal structure from analysis of expanded spread profiles, *Marine Geophysical Researches*, *14* (2), 137-162.

Peate, D.W., C.J. Hawkesworth, M.S.M. Mantovani, and W. Shukowsky, (1990), Mantle Plumes and Flood-Basalt Stratigraphy in the Parana, South-America, *Geology*, *18* (12), 1223-1226.

Planke, S., and O. Eldholm, (1994), Seismic response and construction of seaward dipping wedges of flood basalts - Voring volcanic margin, *Journal of Geophysical Research-Solid Earth*, *99* (B5), 9263-9278.

Planke, S., P.A. Symonds, E. Alvestad, and J. Skogseid, (2000), Seismic volcanostratigraphy of large-volume basaltic extrusive complexes on rifted margins, *Journal of Geophysical Research-Solid Earth*, *105* (B8), 19335-19351.
Plummer, P.S., (1994), Mesozoic source rocks and hydrocarbon potential of the Seychelles offshore, *Journal of Petroleum Geology*, *17* (2), 157-176.
Plummer, P.S., (1996), The Amirante ridge/trough complex: Response to rotational transform rift drift between Seychelles and Madagascar, *Terra Nova*, *8* (1), 34-47.
Randall, G.E., (1989), Efficient calculation of differential seismograms for lithospheric receiver functions, *Geophys. J. Int.*, *99*, 469-481.
Reddy, P.R., (2005), Crustal velocity structure of western India and its use in understanding intraplate seismicity, *Current Science*, *88* (10), 1652-1657.
Richards, M.A., R.A. Duncan, and V.E. Courtillot, (1989), Flood basalts and hot-spot tracks - plume heads and tails, *Science*, *246* (4926), 103-107.
Royer, J.Y., A.K. Chaubey, J. Dyment, G.C. Bhattacharya, K. Shrinivas, V. Yatheesh, and T. Ramprasad, (2002), Paleogene plate tectonic evolution of the Arabian Sea and Eastern Somali Basin, *Sp. Pub. Geol. Soc. Lond.*, *195*, 7-23.
Sandwell, D.T., and W.H.F. Smith, (1997), Marine gravity anomaly from Geosat and ERS-1 satellite altimetry, *J. Geophys. Res.*, *102*, 10039-10054.
Sansom, V., Crustal structure of the NE Seychelles rifted continental margin from geophysical observations, PhD thesis, Imperial College London, 2006.
Shor, G.G., and D.D. Pollard, (1963), Seismic investigations of Seychelles and Saya de Malha Banks, Northwest Indian Ocean, *Science*, *142*, 48-49.
Sleep, N.H., (1997), Lateral flow and ponding of starting plume material, *Journal of Geophysical Research-Solid Earth*, *102* (B5), 10001-10012.
Sleep, N.H., (2007), Edge-modulated stagnant-lid convection and volcanic passive margins, *Geochemistry Geophysics Geosystems*, *8*.
Talwani, M., J.L. Worzel, and M. Landisman, (1959), Rapid gravity computations for two-dimensional bodies with application to the Medocino submarine fracture zone, *J. Geophys. Res.*, *64*, 49-59.
Todal, A., and O. Edholm, (1998), Continental margin off Western India and Deccan Large Igneous Province, *Marine Geophysical Researches*, *20* (4), 273-291.
van Wijk, J.W., R.S. Huismans, M. ter Voorde, and S. Cloetingh, (2001), Melt generation at volcanic continental margins: no need for a mantle plume?, *Geophysical Research Letters*, *28* (20), 3995-3998.
Vogt, U., J. Makris, B.M. O'Reilly, F. Hauser, P.W. Readman, A.W.B. Jacob, and P.M. Shannon, (1998), The Hatton basin and continental margin: Crustal structure from wide-angle seismic and gravity data, *Journal of Geophysical Research-Solid Earth*, *103* (B6), 12545-12566.
Voss, M., and W. Jokat, (2007), Continent-ocean transition and voluminous magmatic underplating derived from P-wave velocity modelling of the East Greenland continental margin, *Geophysical Journal International*, *170* (2), 580-604.
Wegener, A., (1924), *The origins of continents and oceans*, 212 pp., Methuen, London.
White, R.S., (1992a), Crustal structure and magmatism of north-Atlantic continental margins, *Journal of the Geological Society*, *149*, 841-854.
White, R.S., (1992b), Magmatism during and after continental break-up, in *Magmatism and the Causes of Continental Break-up*, edited by B.C. Storey, T. Alabaster, and R.J. Pankhurst, Geological Society Special Publications.
White, R.S., and D. McKenzie, (1989), Magmatism at rift zones: the generation of volcanic continental margins and flood basalts, *Journal of Geophysical Research-Solid Earth*, *94* (B6), 7685-7729.
White, R.S., and D. McKenzie, (1995), Mantle Plumes and Flood Basalts, *Journal of Geophysical Research-Solid Earth*, *100* (B9), 17543-17585.
White, R.S., D. McKenzie, and R.K. O'Nions, (1992), Oceanic crustal thickness from seismic measurements and rare-earth element inversions, *Journal of Geophysical Research-Solid Earth*, *97* (B13), 19683-19715.
White, R.S., T.A. Minshull, M.J. Bickle, and C.J. Robinson, (2001), Melt generation at very slow-spreading oceanic ridges: Constraints from geochemical and geophysical data, *Journal of Petrology*, *42* (6), 1171-1196.
Whitmarsh, R.B., T.A. Minshull, S.M. Russell, S.M. Dean, K.E. Louden, and D.P. Chian, (2001), The role of syn-rift magmatism in the rift-to-drift evolution of the West Iberia continental margin: geophysical observations, in *Non-Volcanic Rifting of Continental Margins: A Comparison of Evidence from Land and Sea*, edited by R.C.L. Wilson, R.B. Whitmarsh, B. Taylor, and N. Froitzheim, pp. 107-124, The Geological Society of London, London.
Whitmarsh, R.B., R.S. White, S.J. Horsefield, J.C. Sibuet, M. Recq, and V. Louvel, (1996), The ocean-continent boundary off the western continental margin of Iberia: Crustal structure west of Galicia Bank, *Journal of Geophysical Research-Solid Earth*, *101* (B12), 28291-28314.
Zelt, C.A., (1999), Modelling strategies and model assessment for wide-angle seismic traveltime data, *Geophysical Journal International*, *139* (1), 183-204.
Zelt, C.A., and P.J. Barton, (1998), Three-dimensional seismic refraction tomography: A comparison of two methods applied to data from the Faeroe Basin, *Journal of Geophysical Research-Solid Earth*, *103* (B4), 7187-7210.
Zelt, C.A., and D.A. Forsyth, (1994), Modeling wide-angle seismic data for crustal structure - southeastern Grenville Province, *Journal of Geophysical Research-Solid Earth*, *99* (B6), 11687-11704.
Zelt, C.A., and R.B. Smith, (1992), Seismic traveltime inversion for 2-D crustal velocity structure, *Geophysical Journal International*, *108* (1), 16-34.
Zhu, L., and H. Kanamori, (2000), Moho depth variation in southern California from teleseismic receiver functions, *J. Geophys. Res.*, *105* (B2), 2969-2980.

11 Figures

Fig.1

(a) Satellite gravity of the north-west Indian Ocean (*Sandwell and Smith*, 1997) showing location of conjugate Seychelles-Laxmi Ridge margin survey lines.

(b) Bathymetry of the Seychelles Plateau and surrounding areas (1 km contour interval, ETOPO5, National Geophysical Data Center, 1993). SP, Seychelles Plateau, MP, Mascarene Plateau. The bold black line marks the Seychelles wide-angle model line presented here and the box marks the area shown in Fig.2. Numbered dark grey circles and dark grey lines are historical sonobuoy wide-angle seismic surveys that determined continental crust beneath the Seychelles Plateau and oceanic crust elsewhere (*Davies and Francis*, 1964; *Francis et al.*, 1966; *Shor and Pollard*, 1963; *Francis and Shor*, 1966). Numbered light grey triangles are DSDP/ODP holes, and unnumbered light grey triangles are commercial holes.

(c) Plate reconstruction using the 27ny Euler rotation pole of *Royer et al.*, 2002 (Lat 18.83^0, Lon 24.86^0 Angle 35.411^0). The Seychelles-Mascarene block is defined by the 1 and 3 km bathymetric contours, the Indian block by the 200 m bathymetric contour and coastline and the Laxmi Ridge (LR) block by gravity data (*Miles and Roest*, 1993). GR, Gop Rift, CR, Indian Continental Rise (*Malod et al.*, 1997). In the reconstruction the Seychelles-Mascarene block is held fixed and the Indian and Laxmi Ridge continental blocks (maintained in their present-day relative positions) are rotated back towards it. The Mascarene plateau (MP) is shown dashed as most, if not all, of it may have formed after break-up (as indicated by ages of recovered volcanics from the holes marked with triangles, *Duncan and Hargraves*, 1990). The white star marks the eruptive centre of the Deccan Traps inferred by *Hooper* (1990), and the dashed circle has a 1000 km radius about this point. The bold black line marks the conjugate pair of velocity models shown in Fig.8.

Fig.2

Bathymetric map of the study area showing locations of shooting tracks and seismic receivers. The bathymetry is a compilation of hull-mounted EM12 swath data and digitised hand-contoured unpublished historical data (R.L. Fisher, pers. comm.). Numbered bold black lines are seismic reflection profiles collected during CD144 (lines 7-21) and fine grey lines are commercial seismic reflection profiles on the plateau. White bars are identified seaward-dipping reflectors from *Collier et al.*, (2008). Black stars are ocean-bottom instruments, black inverted triangles are disposable sonobuoys and white triangles are land seismometer stations. Black dashed lines are the 2D wide-angle model lines. White dotted lines are seafloor spreading anomalies 27n and 28n from *Collier et al.*, (2008).

Fig.3

(a) Migrated stack of part of multi-channel seismic line 9 showing seaward-dipping reflectors (marked with arrows). The data were collected with a 48-channel, 2.4 km long hydrophone streamer simultaneously with the shooting of the main wide-angle. Seabed instruments are marked with numbered triangles.

(b) Migrated stack of the whole of multi-channel seismic line 9. The box marks the area of seaward dipping reflectors (SDRs) shown in detail in (a). The Moho reflection on a neighbouring line can be seen in greater detail in Fig.9a.

(c) Two-dimensional magnetic model of line 9 from *Collier et al.*, (2008). Blocks with natural remanent magnetisation are shaded white/black according to reversed/normal polarity with the intensities given in A/m. The continental crust (shaded light grey) was assigned zero magnetic susceptibility, with all other blocks assigned a susceptibility of 0.04 SI. COB is the continent-ocean boundary. The two seaward-dipping reflector packages (SDRs) identified on the co-incident reflection profile are modelled as weakly magnetised normal polarity bodies. Extending the 60 mm/yr half spreading rate determined for anomalies 26r and 27n up to the COB, implies that most of seafloor spreading anomaly 27r is present, and so the SDRs are inferred to have erupted during chron 28n. The seamount at x=220 km is modelled as a separate, normally-magnetised body because dated samples

recovered from a neighbouring seamount (Darwin Hill, Fig.2) show them not to be contemporaneous with the underlying oceanic crust. The computed ages of the seafloor use the timescale of *Gradstein et al.*, (2005).

Fig.4

The Seychelles plateau crustal structure (a) Velocity-depth profiles obtained from receiver functions (RF, *Hammond et al.*, submitted) and controlled source seismic refraction line 5210 (see Fig.1 for line location). The grey shading shows the range of extended continental crust profiles according to the global compilation of *Christensen and Mooney* (1995). Of the three Seychelles receiver functions, the most reliable is that for Mahé (station 04, as it was calculated from the permanent station with the longest recording window) and the least reliable is that for Denis (station 19, as it is a low-lying coralline cay island with poorer signal-to-noise than the granitic islands of Mahé or Praslin). This range of quality is reflected in the level of detail obtained in the velocity profiles. (b) Ray-traced forward modelling of the *Davies and Francis* (1964) original first arrival travel time picks for line 5210. As the data are un-reversed the model is assumed to be one-dimensional.

Fig.5

Selected record sections with picks (dots with error bars marking assigned uncertainty) and predicted arrivals (lines) overlain (above) and ray-traced model (below). Note that "offset" refers to the separation between the airgun source and the instrument (positive and negative values referring to shots south and north of the instrument respectively) and "distance" refers to the location along the wide-angle model. A reduction velocity of 8 km/s is used throughout. See text for explanation of phase names. The predicted direct arrival curve is included for the seabed sections for reference. Seabed multiples are labelled m. The seabed record sections are of the hydrophone component, and the land record sections the vertical geophone. (a) OBS35, (b) OBS48 (c) OBH54 (d) OBH57 (e) OBH61 (f) OBH64 (g) landstation 19 (Denis Island) (h) landstation 4 (Mahé Island).

Fig.6

(a) Final P-wave velocity model with model layer boundaries. Instrument positions are indicated with numbered triangles. The Mahé (station 04), Praslin (station 10) and Denis (station 19) receiver-function velocity profiles and re-modelled east-west controlled source profile 5210 are marked for reference.

(b) Diagonal of the resolution matrix for the model velocity nodes shown as a contour plot. A value of 1 indicates full resolution, but for real data a value above 0.5 is considered acceptable (*Zelt*, 1999). Note that there is a trade off between resolution and node spacing, which accounts for the apparent low resolution of the sediment layer which has dense node spacing defined from the seismic reflection data (and hence not taken into account in the calculation of the resolution). Also shown are the ray paths for the top (PtP) and bottom underplate (PbP) reflections from the transitional and continental parts of the model.

(c) Velocity-depth profiles at various points across the model. The vertical scale is depth below top basement. The oceanic profiles (x=800, 160 and 240 km) are compared to the envelope of values for 29-140 Ma old Pacific Ocean crust from *White et al.*, (1992) (grey shading).

Fig.7

Gravity model (below – densities in g/cm^3) and calculated response (above). Cross-over error analysis with historical ship tracks suggests an error of ± 5 mGal on the observed free-air gravity anomaly. The model layer boundaries are defined directly from velocity contours of the final velocity model (Fig.6) without any adjustment. The sediments were defined by two blocks, with densities were assigned according to their mean seismic velocity and the empirical velocity-density relationship of *Ludwig et al.*, (1970). The crust was defined by three blocks, with the densities assigned using the relationship $\rho=0.989 + 0.289Vp$, from the linear-solution to a global compilation of igneous and metamorphic rocks by *Christensen and Mooney* (1995). The mantle was defined by a single block. We found that in order to model the long wavelength (>200 km) gravity anomaly we needed to assign a relatively low density of 3.15 kg/m^3 to the mantle layer. We did not attempt to model the mantle structure in greater detail due to unknown contributions to the observed gravity deeper or outside the region constrained by the wide-angle data, but note that a low density in the lithospheric mantle beneath the plateau was predicted from

945 the Mahé receiver function which showed it to have a P-wave velocity of just 7.7 km/s (Fig.4a). Note
946 that as the model is two-dimensional short-wavelength (< 50 km) features such as seamounts in deep
947 water and sedimentary basins on the plateau will be over-estimated if they are crossed by the profile
948 and under-estimated if they lie off-line.

949
950 **Fig.8**
951 Seismic structure of the conjugate Seychelles-Laxmi Ridge margins (below), with magnetic model for
952 the Laxmi Ridge margin (*Collier et al.*, 2008) above. Both margins were surveyed during a single
953 cruise using the same experimental techniques. The Laxmi Ridge margin data were modelled
954 independently but using the same methods as described here (*Lane,* 2006; *Minshull et al.*, 2008).

955
956 **Fig.9**
957 (a) Multichannel seismic line 13 and line drawing showing the best-imaged seaward-dipping reflector
958 package from the north Seychelles margin. (b) Line drawing of SDRs at the north Atlantic Edoras Bank
959 margin from *Barton and White* (1997). Note the different plot scales, and much more extensive SDR
960 development at the distal North Atlantic margin.

961
962 **Fig.10**
963 Locations of selected previous passive margin seismic experiments detailed in Table 2. Individual
964 seismic profiles are marked with black lines, with reference numbers in brackets indicating margins
965 defined in Table 2 as "non-volcanic" or "intermediate". The stars mark the Seychelles-Laxmi Ridge
966 study areas. Large Igneous Provinces from *Coffin and Eldholm* (1994) are shaded black and hotspots
967 linked with continental break-up and plume tail offshore ridges discussed in the text are labelled IC =
968 Iceland, TC = Tristan da Cunha and RE = Réunion. The yellow circles with black centres mark the
969 assumed positions of the Iceland and Tristan da Cunha hotspots at the time of continental break-up
970 used to calculate the plume-offset distances in Table 2. Seafloor spreading rates are from *Muller et al.*,
971 (2008).

972
973 **Fig.11**

(a) Relationship between thickness of the earliest-formed oceanic crust with plume distance for the selected volcanic margins of the North (closed circles) and South (open circles) Atlantic. The margin reference numbers refer to those given in Table 2. Best-fitting straight lines for the two regions are shown, together with their R^2 correlation coefficients. Note how the oceanic crustal thickness formed at the north Seychelles margin is significantly thinner than all other volcanic margins formed at similar distances to the Iceland and Tristan da Cunha plumes.

(b) Relationship between thickness of the earliest-formed oceanic crust and margin width. Again, the margin reference numbers refer to those given in Table 2. North Atlantic margins are shown with closed circles; South Atlantic margins open circles; and all other margins diamonds. Only profiles for which full continental crust thickness was achieved on the profile are plotted. The best-fitting straight line is shown, but note the low R^2 correlation coefficient.

(c) Predicted average oceanic crustal velocity versus thickness according to the model of *Holbrook et al.*, (2001). Two scenarios are shown, passive upwelling alone (χ=1, parameterised according to the melting models of *McKenzie and Bickle*, 1988 and *Langmuir et al.*, 1992) and active upwelling (with active to passive upwelling ratios χ of 2 and 4). Dashed lines are mantle potential temperature for the McKenzie & Bickle melting model. According to this model the Seychelles oceanic crust was formed by passive upwelling only of a non-hot mantle. Results for the distal SE Greenland margins (numbered as per Table 2) and East Pacific Rise at 17^0 S from *Holbrook et al.*, (2001) are shown for comparison.

(d) Relationship between initial oceanic crustal thickness and seafloor spreading rate. Margin symbols as in (b). For clarity only the non-Atlantic margins are numbered according to the listing in Table 2. The inverted triangles mark a global compilation of the thickness of "normal" oceanic crust (i.e. measured away from the immediate passive margin zone, plume traces and fracture zones) by *Bown and White* (1994) as updated by *White et al.*, (2001) and *Minshull et al.*, (2001). The dashed lines show the predicted steady-state oceanic crustal thickness according to the passive melting model of *Bown and White* (1994).

12 Tables

Table 1

Numbers of observations (n), average pick uncertainty (t_{unc}), average root-mean-square travel-time misfit (t_{RMS}) and normalised travel-time misfit (χ^2) for individual phases. If χ^2 = 1 the model is a statistically perfect fit to the data given the assigned travel-time pick uncertainties. Code refers to the standard rayinvr assignments, n.m, where n is the deepest layer traversed by the ray, and m is 1 for a turning ray, 2 for a reflection and 3 for a refraction. PcP=basement reflection (including artificial zero-offset picks made from the co-incident reflection profile), Ps=sediment layer turning ray, Pg1-3= crustal layer turning rays, PmP=Moho reflection (including artificial zero-offset picks made from the co-incident reflection profile), Pn=mantle refraction, Pu=underplate turning rays, PtP=top underplate reflection, PbP=bottom underplate reflection.

Table 2

Compilation of results from other studies of continental rifted margins. See Fig.10 for survey locations. The margins are classified according to features within the continent-ocean transition: v- volcanic if they display thick SDRs and underplate; nv- non-volcanic if they display tilted fault blocks and serpentinised mantle; and int- intermediate if they do not readily fall into the other two categories. The distance to hotspot centre in the North and South Atlantics are measured from the point on the profile of the first oceanic crust to the centre of the oldest parts of the Greenland-Iceland-Faeroe Ridge, Rio Grande Rise and Walvis Ridge (as marked with the yellow circles in Fig.10). Where full thickness continental crust was not achieved on the wide-angle profile the measured margin width is marked with a '>'. The onset seafloor spreading rate was extracted from the digital grid of *Muller et al.*, (2008) (Fig.10). In a few cases we needed to use a rate from up to 20km ocean-ward of our actual oceanic crust thickness measurement point. We rejected some seismic profiles from our compilation at this stage (for example around Antarctica) if an associated seafloor spreading rate was not available.

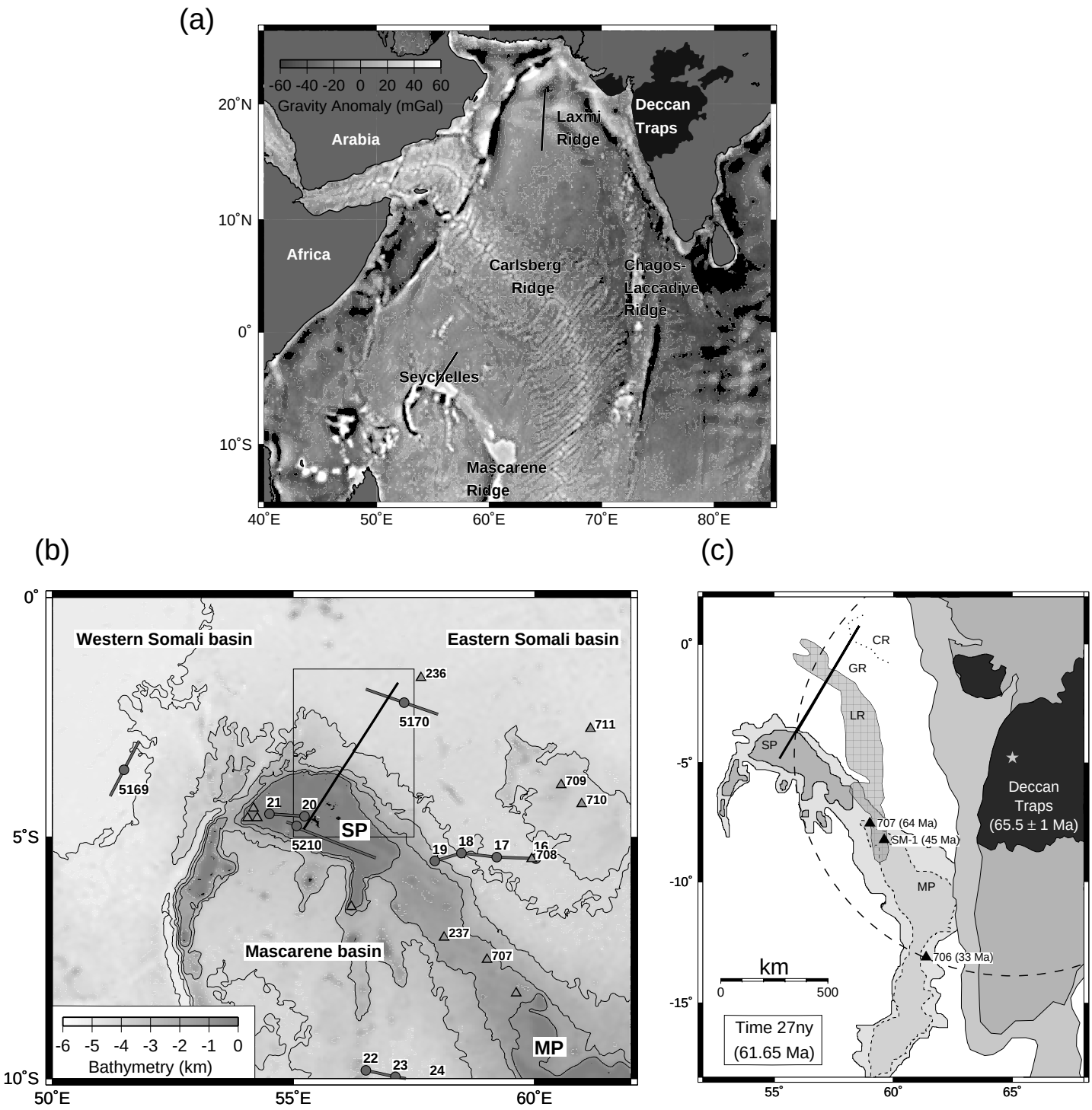

Collier et al. Fig.1

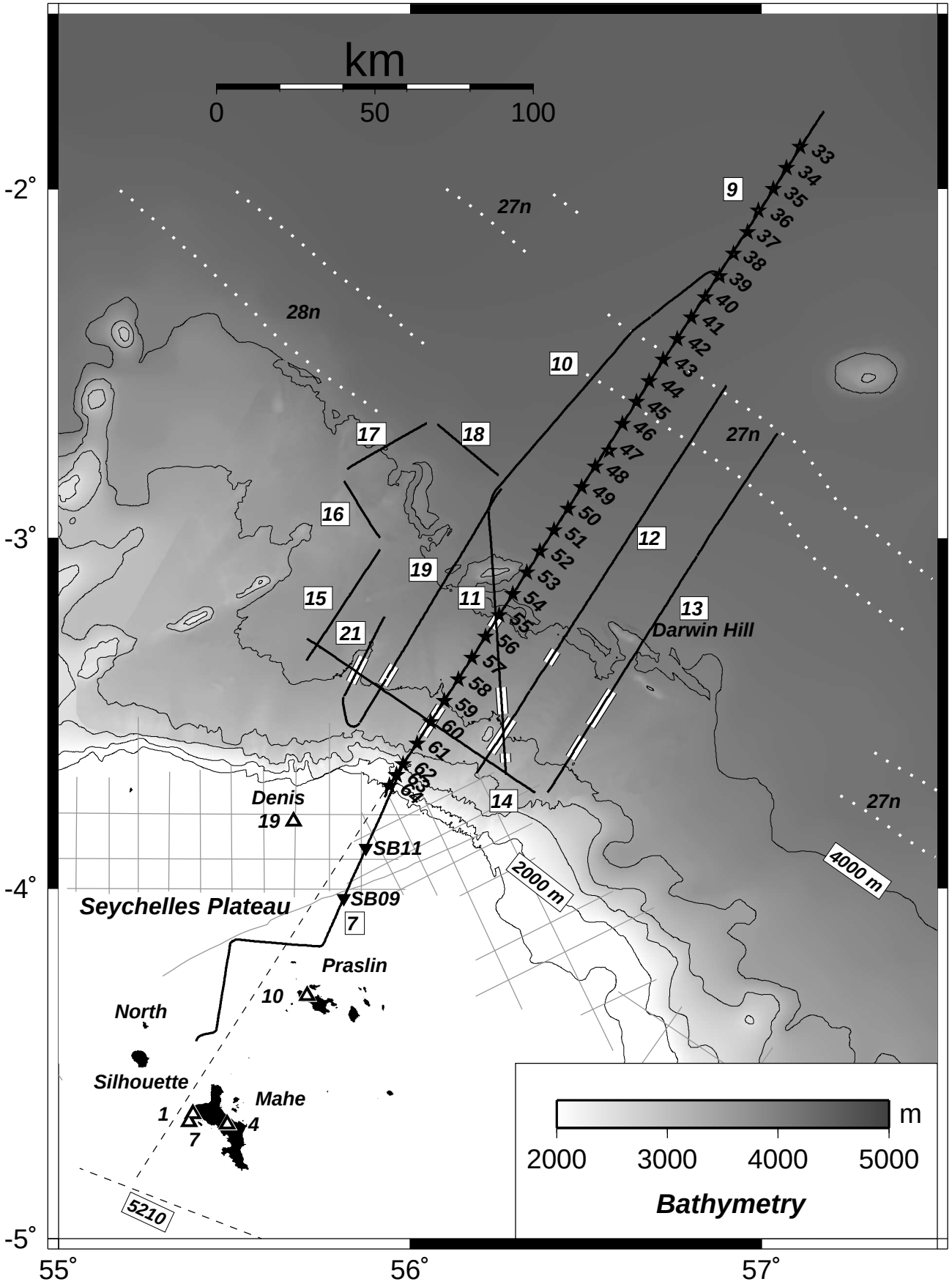

Collier et al Fig.2

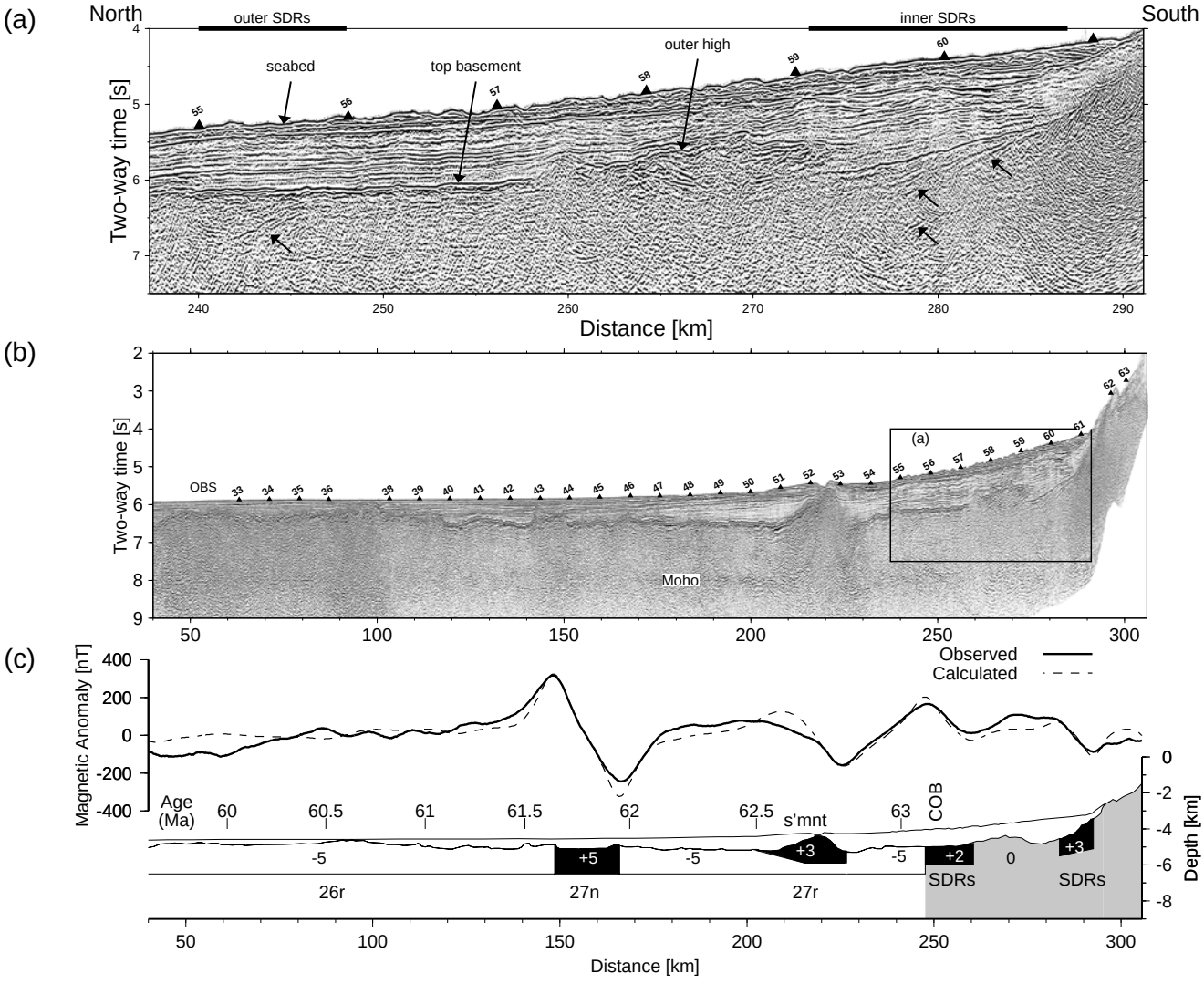

Collier et al. Fig.3

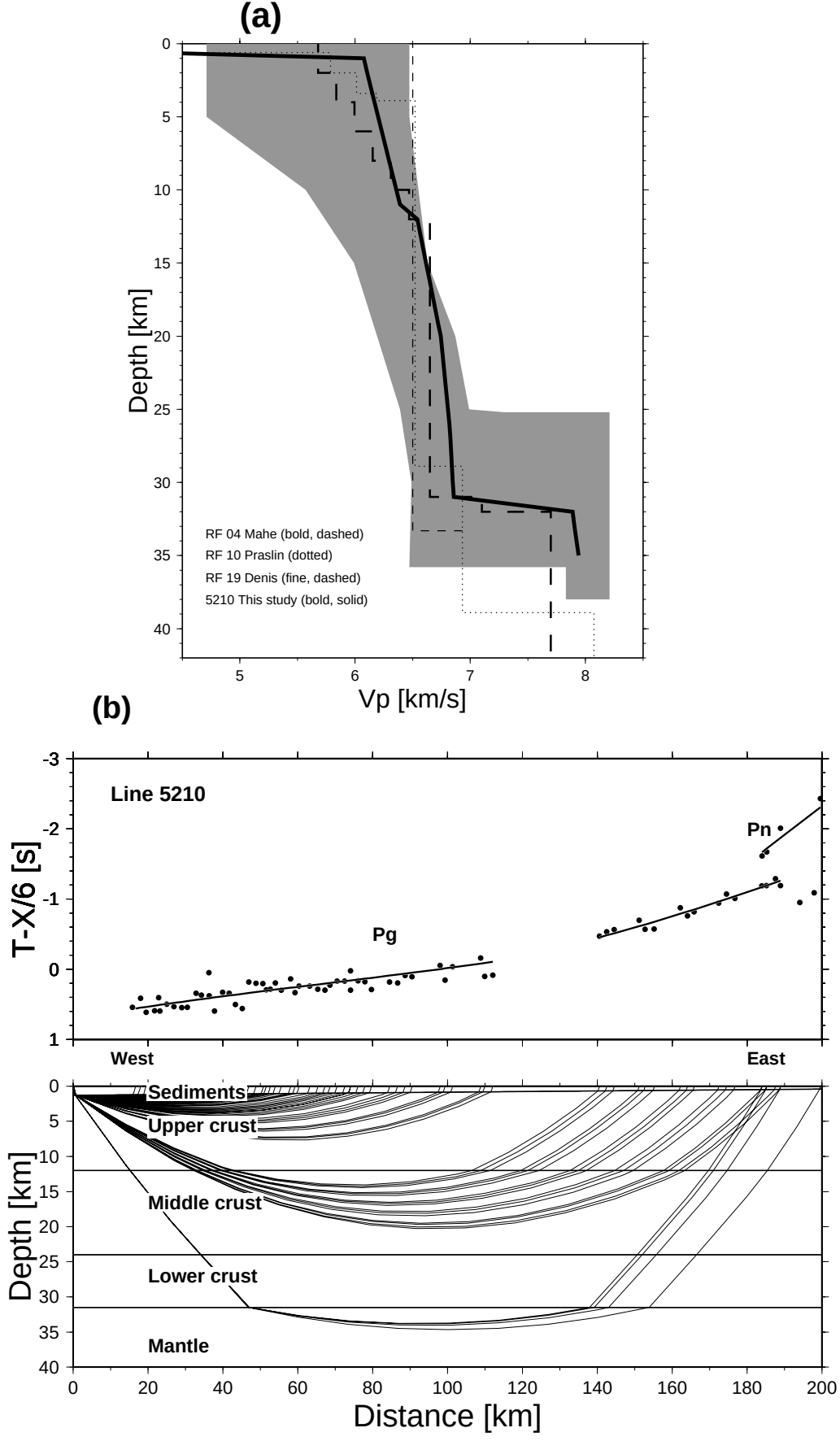

Collier et al. Fig.4

(a)

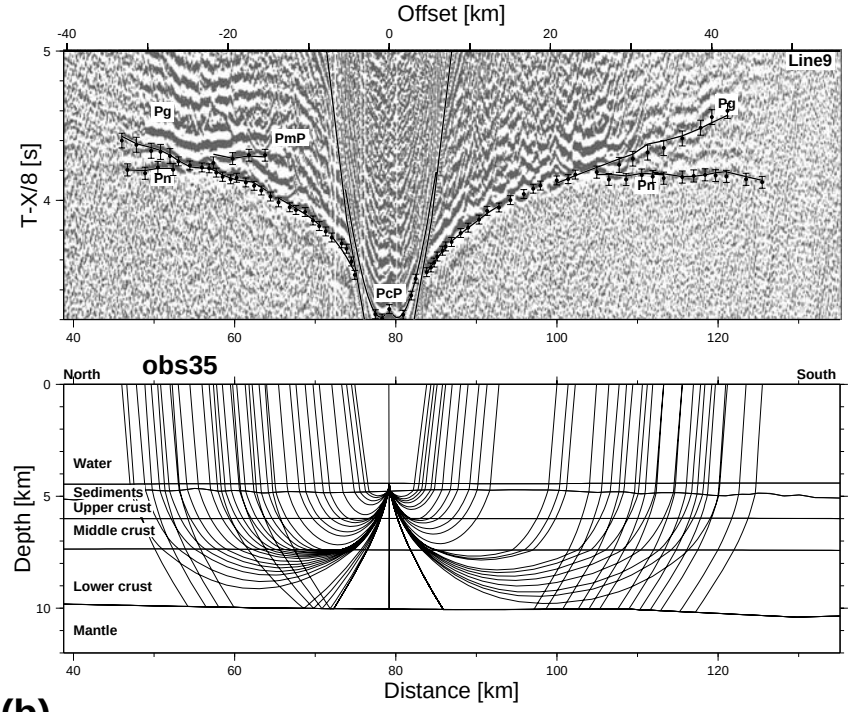

(b)

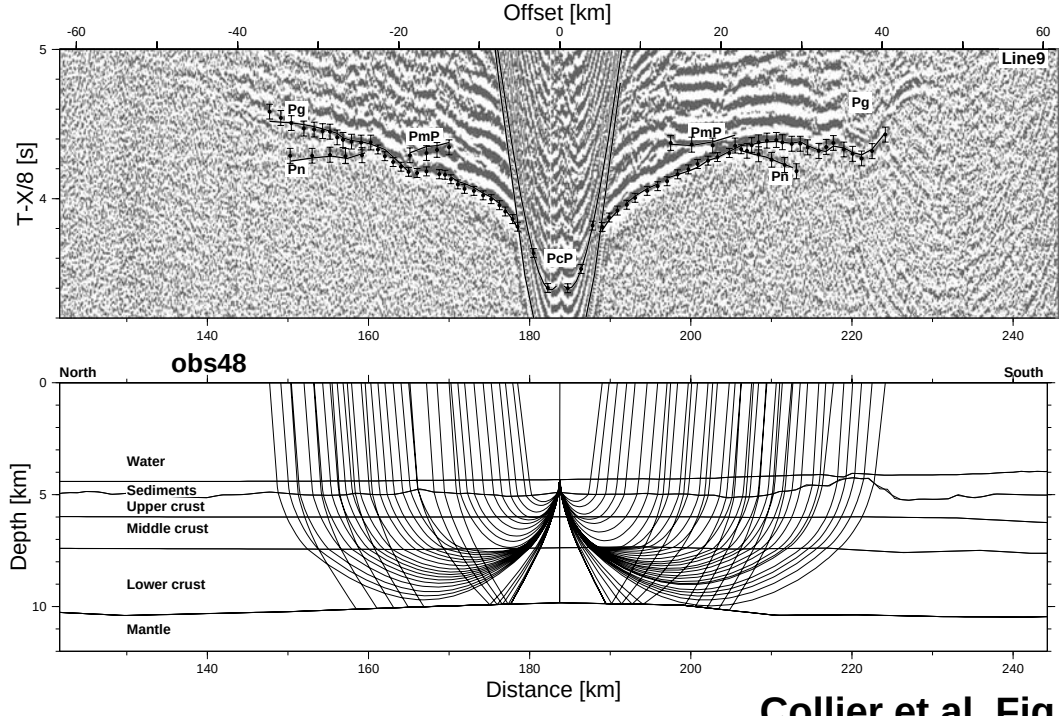

Collier et al. Fig.5

(c)

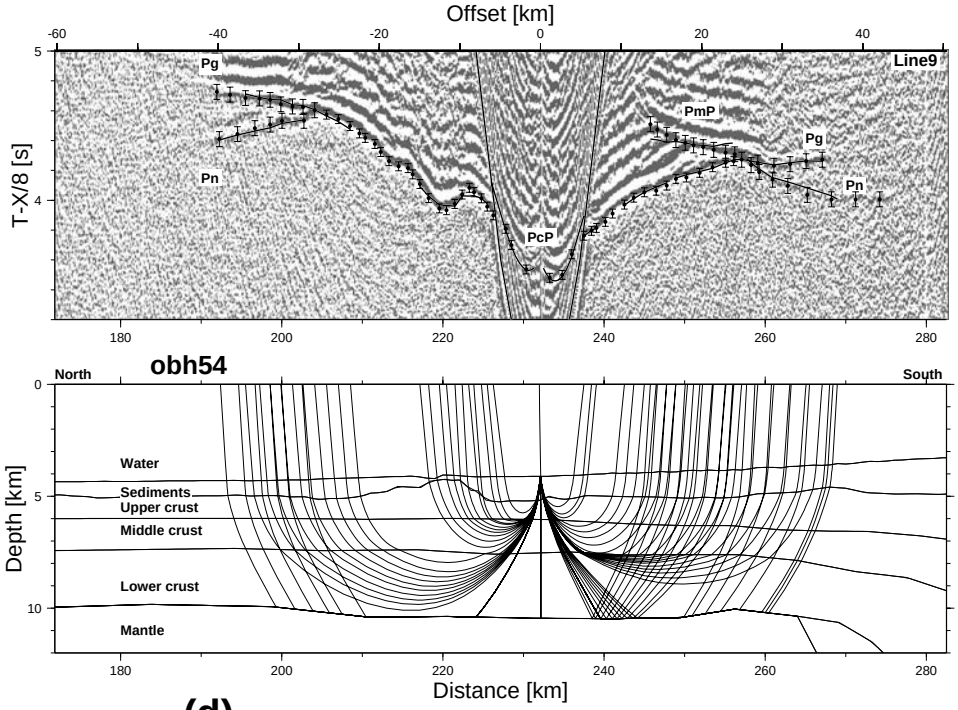

(d)

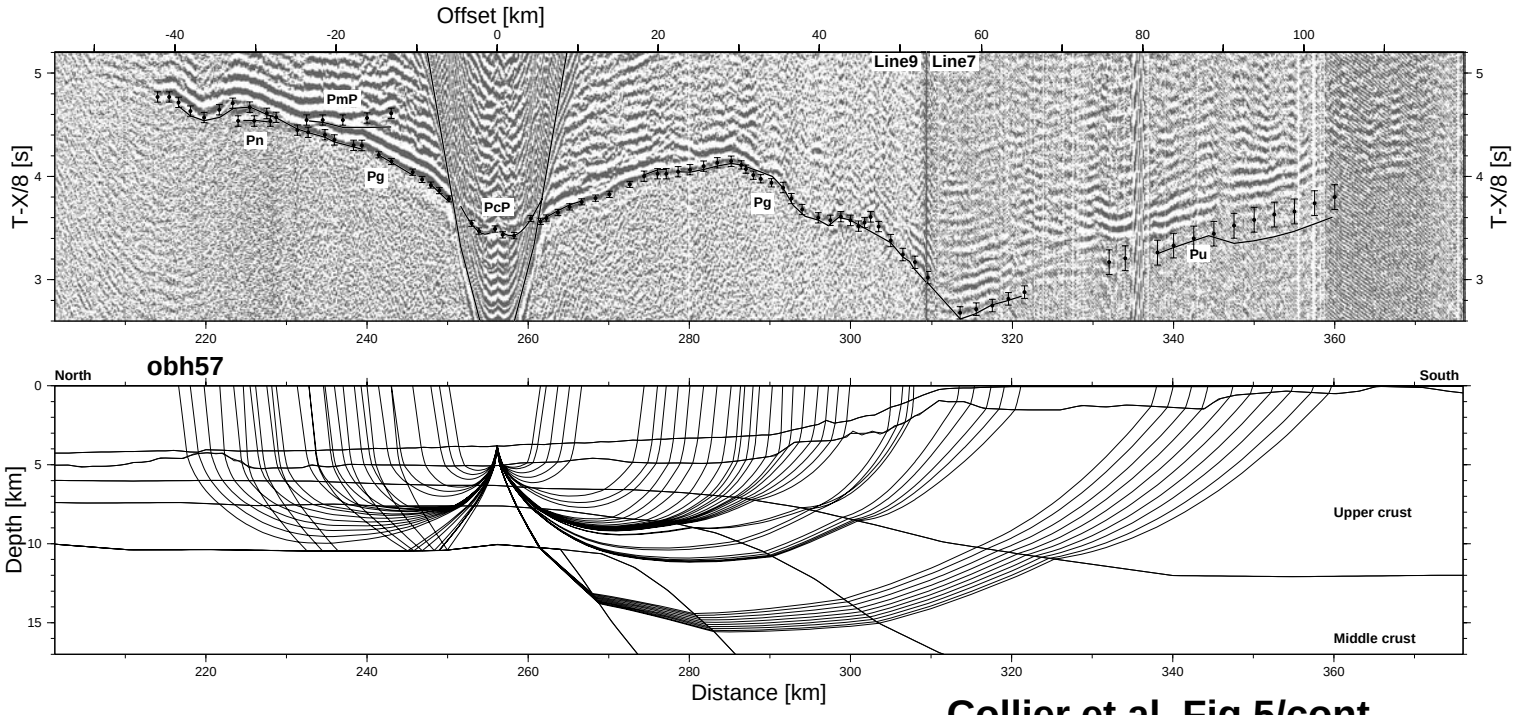

Collier et al. Fig.5/cont

(e)

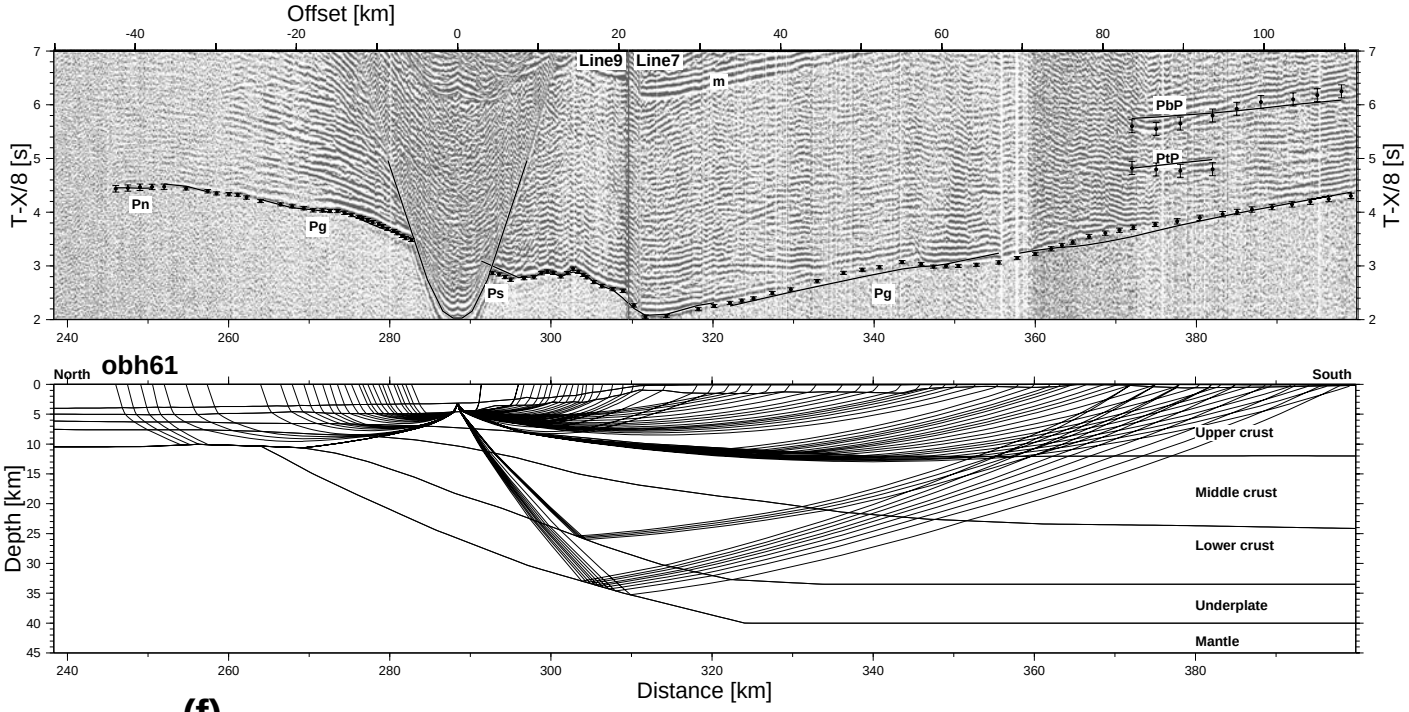

(f)

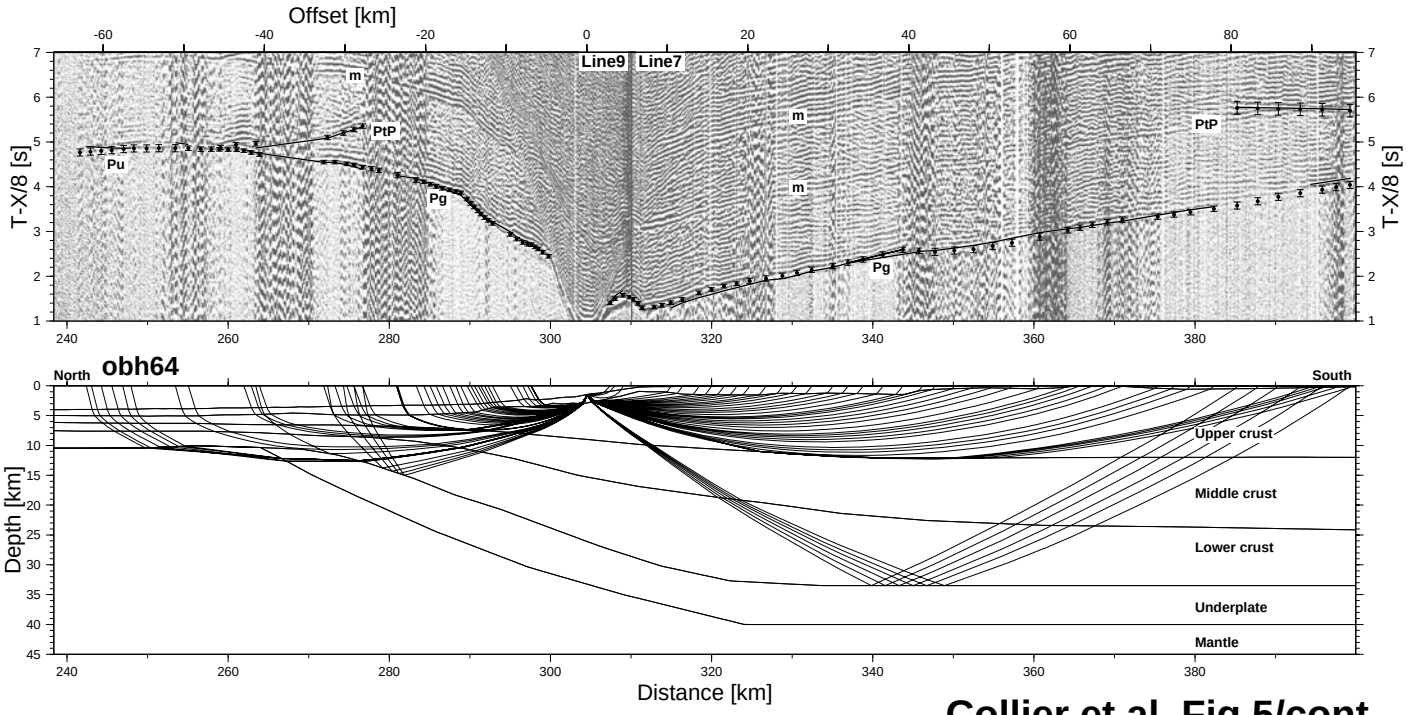

Collier et al. Fig.5/cont

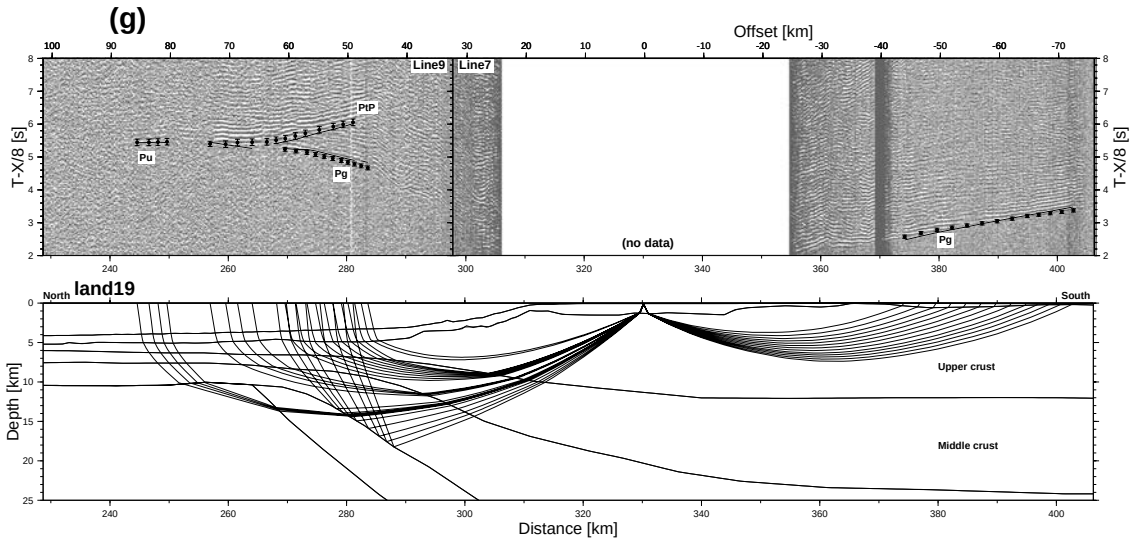

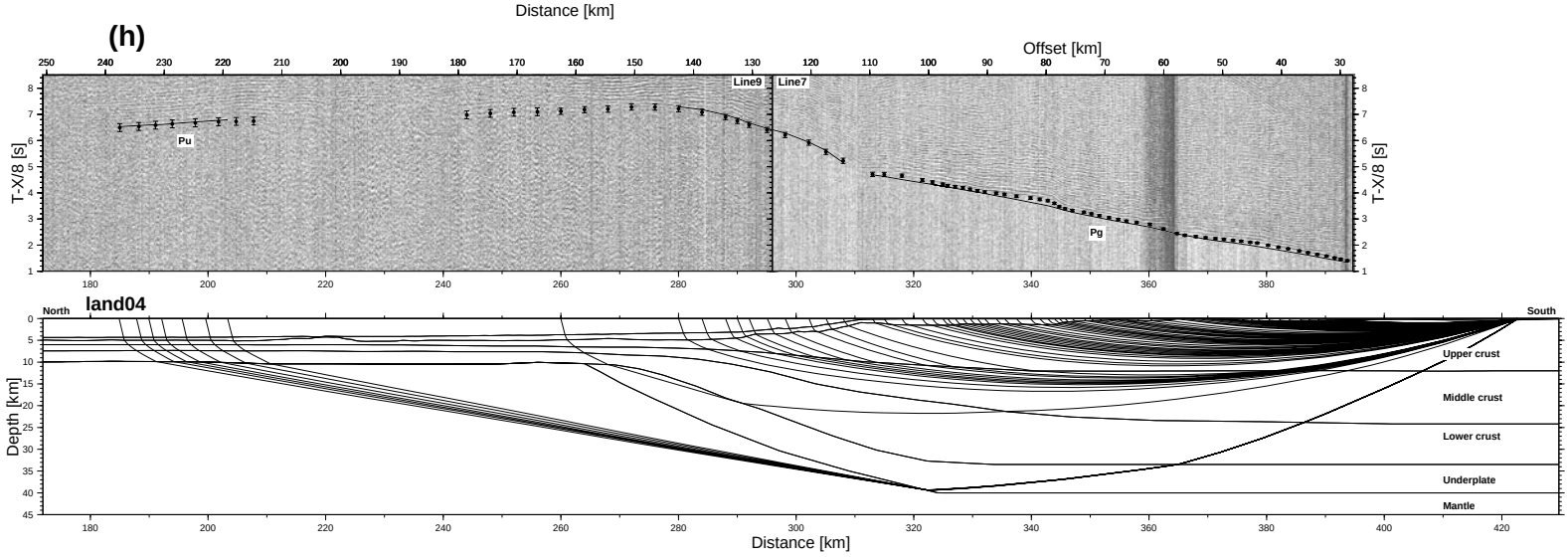

Collier et al. Fig.5/cont

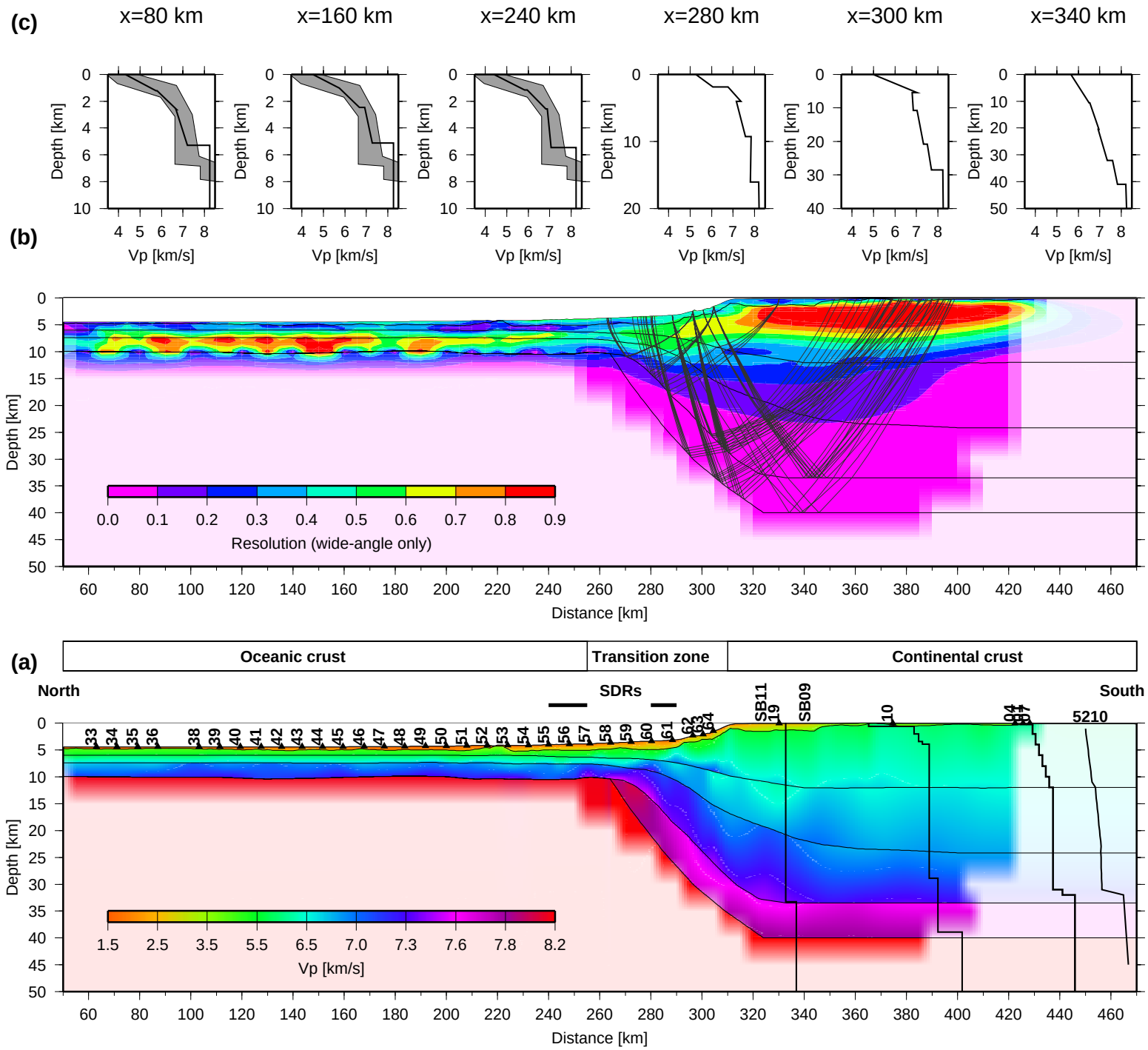

Collier et al. Fig.6

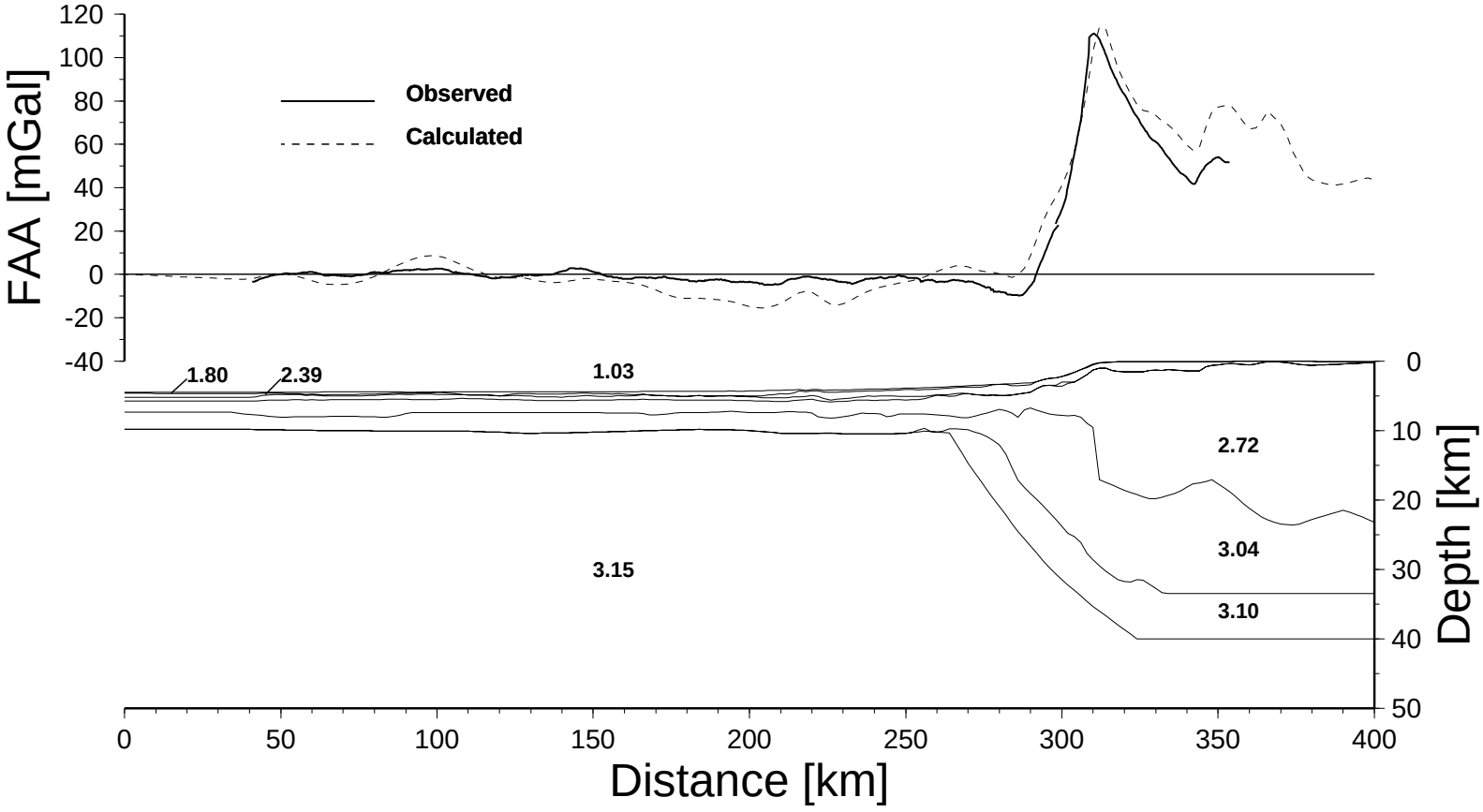

Collier et al. Fig.7

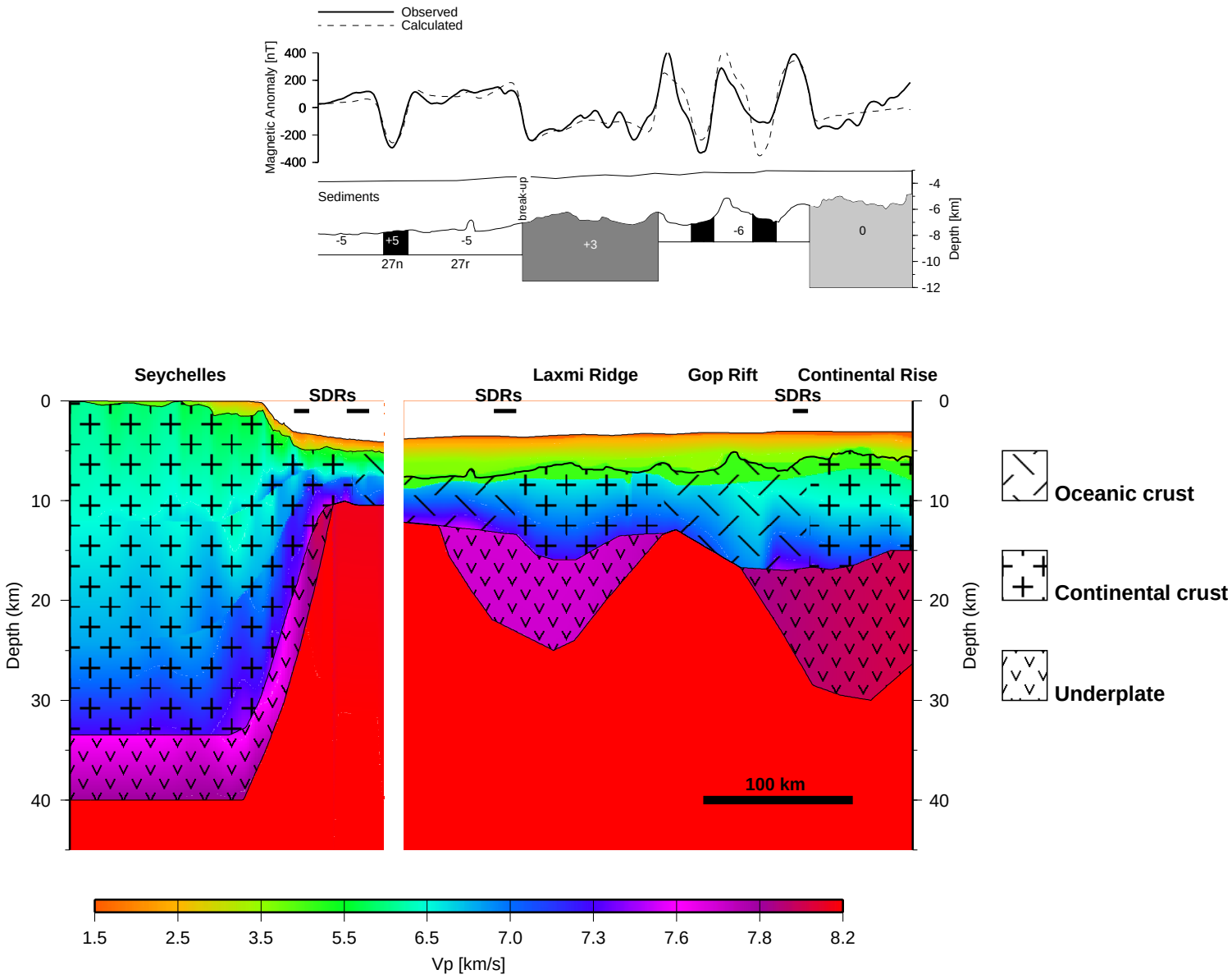

Collier et al. Fig.8

(a)

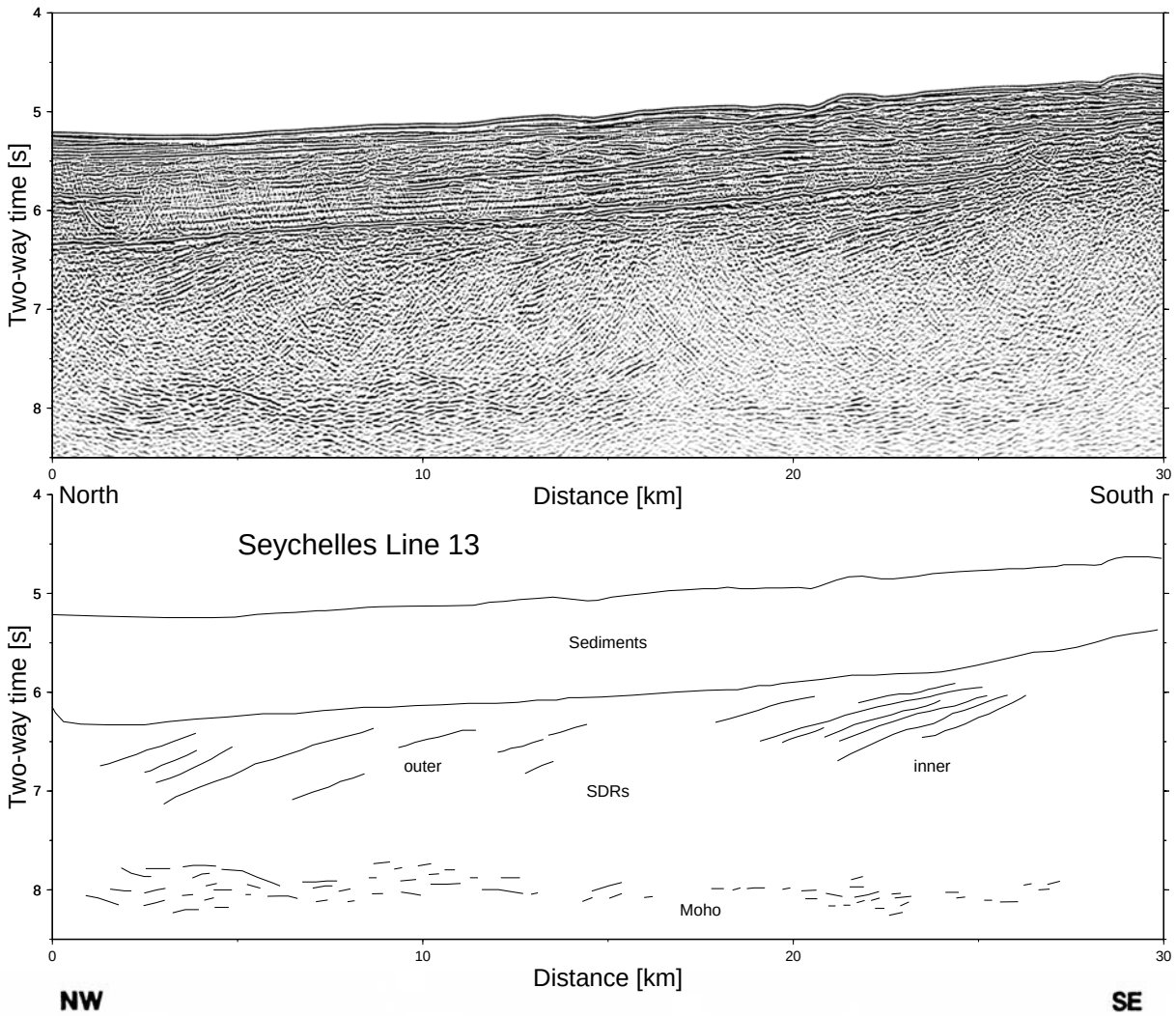

(b)

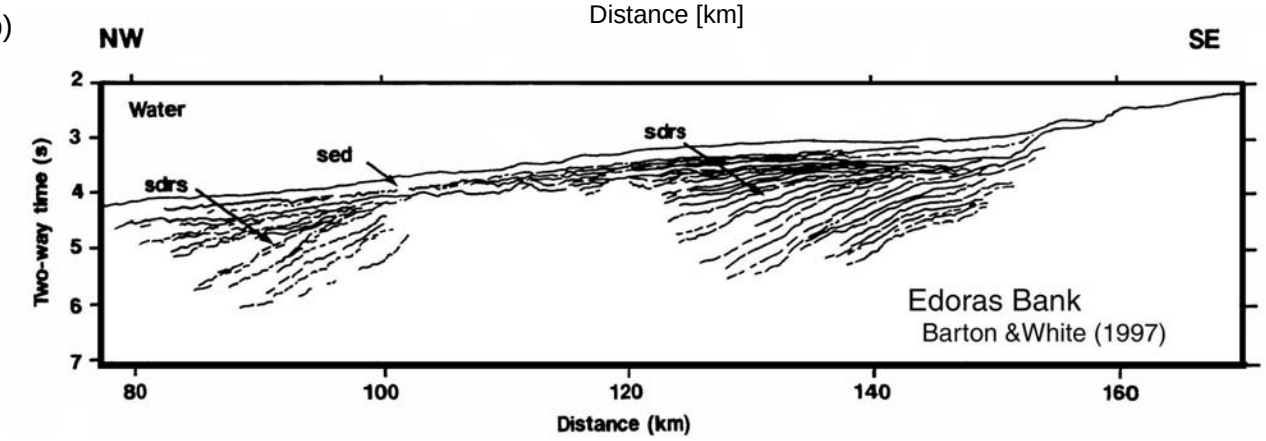

Collier et al. Fig.9

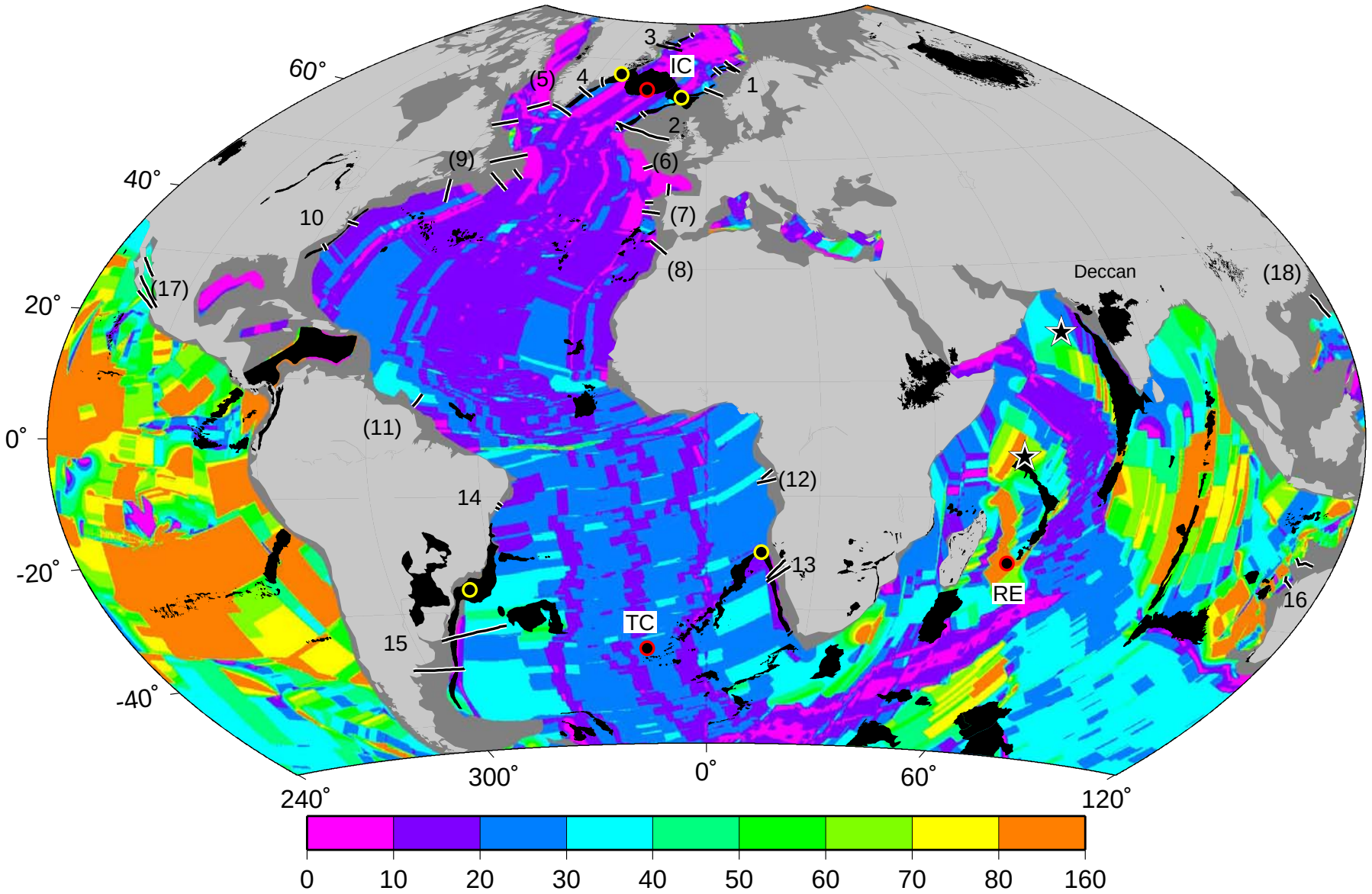

Collier et al. Fig.10

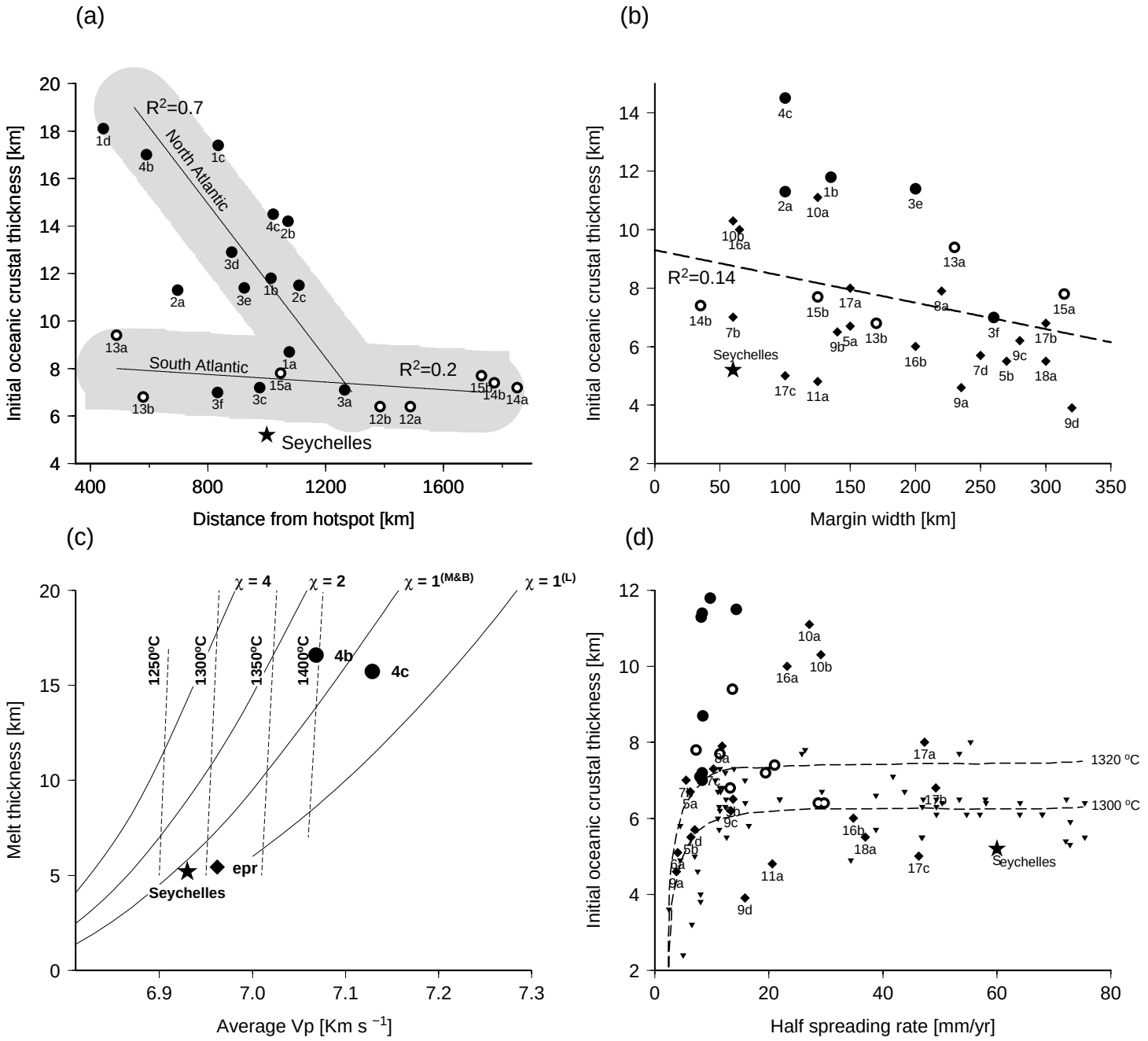

Collier et al. Fig.11

Collier et al., Table 1. Model results summary.

Phase	**Code**	**n**	**t_{unc} (s)**	**t_{RMS} (s)**	**χ^2**
PcP	2.2	94	0.030	0.013	0.201
Ps	2.1	22	0.073	0.092	2.368
Pg1	3.1	486	0.043	0.050	1.334
Pg2	4.1	313	0.036	0.039	0.629
Pg3	5.1	785	0.041	0.039	0.868
PmP	5.2	207	0.060	0.055	0.845
Pn	6.3	261	0.048	0.028	0.329
Pu	7.1	44	0.088	0.118	2.197
PtP	5.2	39	0.065	0.074	0.711
PbP	6.2	21	0.147	0.222	2.035
All		2272		0.050	0.890

Collier et al., Table 2. Compilation of results from other studies of continental rifted margins.

Province	Reference number	Margin name	Reference	Wide-angle Profile id	Data	Type	Lon	Lat	Distance to hotspot centre	Earliest oceanic crust thickness	Margin width[1]	Onset seafloor half spreading rate
									[km]	[km]	[km]	[mm/yr]
	Star	Seychelles	This study	Line-9+7	OBS	int	56	-3	1000	5.2	65	60.0
North Atlantic	1a	Lofoten	Goldschmidt-Rokita et al., 1994	LM-1A	OBS	v	9.5	69.1	1076	8.7	>120	8.4
	1b	Lofoten - south	Mjelde et al., 1992	Line-3	OBS	v	8.2	68.8	1014	11.8	135	9.7
	1c	Voring	Mjelde et al., 2005	Obs99	OBS	v	3.8	68.2	834	17.4	>105	9.4
	1d	Møre	Olafsson et al., 1992	MVM-1	ESP	v	0.1	64.1	444	18.1	340	12.6
	2a	Hatton Bank	Fowler et al., 1989	N18	ESP	v	-19.3	59.4	697	11.3	100	8.1
	2b	Hatton Bank - south	Vogt et al., 1998	RAPIDS	OBS	v	-23.4	56.7	1072	14.2	400	14.3
	2c	Edoras	Barton and White, 1997	Cam77	OBS	v	-24.0	56.6	1109	11.5	>80	14.3
	3a	NE Greenland	Mutter and Zehnder, 1988	COP-39,40	ESP	v	-7.2	75.5	1264	7.1	>70	7.9
	3c	NE Greenland	Mutter and Zehnder, 1988	COP-46	ESP	v	-14.9	73.8	976	7.2	>55	8.3
	3d	NE Greenland	Mutter and Zehnder, 1988	COP-61	ESP	v	-16.1	72.9	880	12.9	>115	8.7
	3e	NE Greenland	Voss and Jokat, 2007	400	OBS	v	-16.7	73.7	923	11.4	200	8.3
	3f	NE Greenland	Voss and Jokat, 2007	500	OBS	v	-18.0	72.9	832	7.0	260	8.3
	4a	SE Greenland	Holbrook et al., 2001	Sigma-II	OBS	v	-35.9	64.7	321	28.0	160	12.7
	4b	SE Greenland	Holbrook et al., 2001	Sigma-III	OBS	v	-39.0	62.7	591	17.0	120	14.8
	4c	SE Greenland	Holbrook et al., 2001	Sigma-IV	OBS	v	-42.2	59.1	1022	14.5	100	13.3
	5a	SW Greenland	Chian and Louden, 1994	88R2	OBS	nv	-50.0	60.0	n/a?	6.7	150	6.2
	5b	Labrador	Chian et al., 1995	90R1	OBS	nv	-56.2	56.2	n/a?	5.5	270	6.3
Central Atlantic	6a	Goban Spur	Bullock and Minshull, 2005	WAM	OBS	nv	-14.5	48.5	n/a	5.1	>100	4.0
	7b	Biscay	Fernandez-Viejo et al., 1998	IAM-12	Land	int	-8.8	44.5	n/a	7.0	60	5.5
	7c	Galicia Bank	Whitmarsh et al., 1996	Line-6	OBS	nv	-13.0	42.1	n/a	7.3	>150	10.3
	7d	Iberia	Dean et al., 2000	IAM-9	OBS	nv	-13.0	40.5	n/a	5.7	250	7.0
	8a	Moroccan	Contrucci et al., 2004a	Profile-4	OBS	nv	-10.5	34.3	n/a	7.9[2]	220	11.8
	9a	Orphan Basin	Chian et al., 2001	86-6(8)	OBS	nv	-44.5	50.3	n/a	4.6	235	3.8
	9b	Flemish Cap	Funck et al., 2003	Screech-1	OBS	nv	-43.5	46.4	n/a	6.5	140	13.7
	9c	Grand Banks	Lau et al., 2006	Screech-3	OBS	nv	-46.0	44.0	n/a	6.2	280	13.3
	9d	Nova Scotia	Funck et al., 2004	Smart-1	OBS	nv	-58.0	42.7	n/a	3.9	320	15.8
	10a	Baltimore Trough	Holbrook et al., 1994a	EDGE -801	OBS	v	-74.0	36.4	n/a?	11.1	125	27.1
	10b	Carolina Trough	Holbrook et al., 1994b	BA-6	OBS	v	-76.5	31.7	n/a?	10.3	60	29.1
	11a	Guiana	Greenroyd et al., 2007	Profile-A	OBS	int	-51.0	6.0	n/a	4.8	125	20.6
South Atlantic	12a	Congo	Contrucci et al., 2004b	Profile-14	OBS	int	10.2	-6.4	1487	6.4	>170	29.7
	12b	Angola	Contrucci et al., 2004b	Profile-7+11	OBS	int	10.5	-7.4	1385	6.4	>135	28.7

	13a	Namibia	Bauer et al., 2000	Transect-1	OBS	v	11.9	-23.8	489	9.4	230	13.6
	13b	Namibia - south	Bauer et al., 2000	Transect-2	OBS	v	11.9	-24.7	580	6.8	170	13.2
	14a	Brazilian	Mohriak et al., 1998	Profile-A	MCS +gravity	v	-36.3	-11.6	1850	7.2	>70	19.4
	14b	Brazilian	Mohriak et al., 1998	Profile-C	MCS +gravity	v	-36.8	-12.1	1773	7.4	35	21.0
	15a	Uruguay	Chang et al., 1992	Profile-B	Sonobo uys	v	-50.4	-34.3	1047	7.8	314	7.2
	15b	Argentine	Franke et al., 2006	BGR98-01	OBH	v	-53.3	-40.0	1729	7.7	125	11.4
West Australia	16a	Cuvier	Hopper et al., 1992	Line-670	ESP	v	111.6	-22.2	n/a	10.0	65	23.2
	16b	Exmouth plateau	Mutter and Larson, 1989	Line-652	ESP	int	111.7	-18.7	n/a	6.0	200	34.8
West America	17a	Gulf of California	Lizarralde et al., 2007	Segment G	OBS	int	-111.6	27.4	n/a	8.0	150	47.3
	17b	Gulf of California	Lizarralde et al., 2007	Segment A	OBS	int	-109.0	22.8	n/a	6.8	300	49.3
	17c	Gulf of California	Lizarralde et al., 2007	Segment C	OBS	int	-109.1	24.0	n/a	5.0	100	46.3
SE Asia	18a	China	Nissen et al., 1995	Eastern	ESP	int	118.6	18.6	n/a	5.5	300	36.9

[1]a > symbol means that full thickness continental crust is not achieved on the profile (defined as a thickness of more than 25 km unless data suggests a smaller value was acceptable) and so the measured width is a minimum bound estimate

[2]this may overprinted with late Cenozoic volcanism and the original oceanic crust may have been thinner